# Why Shallow Networks Struggle with Approximating and Learning High Frequency: A Numerical Study

**Shijun Zhang**[*]
Department of Mathematics
Duke University
shijun.zhang@duke.edu

**Hongkai Zhao**[*]
Department of Mathematics
Duke University
zhao@math.duke.edu

**Yimin Zhong**[*]
Department of Mathematics and Statistics
Auburn University
yzz0225@auburn.edu

**Haomin Zhou**[*]
School of Mathematics
Georgia Institute of Technology
hmzhou@math.gatech.edu

## Abstract

In this work, a comprehensive numerical study involving analysis and experiments shows why a two-layer neural network has difficulties handling high frequencies in approximation and learning when machine precision and computation cost are important factors in real practice. In particular, the following fundamental computational issues are investigated: (1) the best accuracy one can achieve given a finite machine precision, (2) the computation cost to achieve a given accuracy, and (3) stability with respect to perturbations. The key to the study is the spectral analysis of the corresponding Gram matrix of the activation functions which also shows how the properties of the activation function play a role in the picture.

## 1 Introduction

Neural networks are now widely used in machine learning, artificial intelligence, and many other areas as a parameterized representation with certain structures for approximating an input-to-output relation, e.g., a function or map in mathematical terms. It has met with a lot of success as well as challenges in practice. More importantly, many basic as well as practical questions are still open. Extensive study has been carried out to understand the properties of neural networks and how they work in different perspectives, such as universal approximation property, representation capacity, and optimization process (mostly based on gradient descent with different variations), often separately. For example, it has been widely known that neural networks can approximate any Lipschitz function with a small error. The approximation theory has been extensively studied for various types of activation functions and diverse structures of networks [1, 5, 6, 8, 10, 15, 19, 22, 30, 31, 32, 33, 34, 36, 41, 42, 45, 46, 47]. Recently, there are works [31, 42, 44] discussing the explicit constructions of the "optimal" networks of multiple layers. However, one daunting issue that has not been studied systematically in the past is whether such "optimal" approximations can be possibly attained by training the networks and more importantly, given a finite machine precision and computational cost, what is the best result one can get. Hence an effective algorithm needs to consider all these aspects to achieve well-balanced accuracy, efficiency, and stability. Due to the nonlinear nature of neural network representations, this is a very challenging task.

In this work, we study a few basic and important questions from a numerical analysis perspective for two-layer neural networks: (1) the best accuracy one can achieve given a finite machine precision; (2) the minimum computation time (cost) to achieve a given accuracy for the training process; and

[*]Equal contribution.

(3) stability to perturbations, e.g., noise in the data, or over-fitting. Our study shows that a shallow neural network is essentially a "low-pass filter" or "regularizer" due to the form of neural network representation and finite computation resources, e.g., machine precision, computation cost, in practice. These understandings propose the study of similar but more challenging questions for deep neural networks.

Our main contributions are summarized here:

- We analyze the spectral properties of the Gram matrix corresponding to activation functions. The spectral analysis shows that a two-layer neural network is essentially a low-pass filter and how machine precision and different activation functions affect the low-pass filter.
- We investigate the learning dynamics for gradient flow-based methods. The stiffness of the system, characterized by the spectral analysis, causes slow learning dynamics for high-frequency modes and long training time to reach (if possible) the optimal solution in practice.
- We characterize the Rashomon set for two-layer neural networks. The result reveals why oscillatory functions are difficult to represent and learn from a probability perspective.

In particular, our study shows rapid decay in eigenvalues of the Gram matrix due to strong correlations among the activation functions as the basis of representation. Such decay phenomenon has been also studied in [14] in a special discrete setting in one dimension. As a consequence of the ill-conditioning of the Gram matrix, only leading modes, the number of which depends on the spectral decay rate of the Gram matrix and machine precision, can be resolved and stably used for approximation, a low-pass filter in this sense. Although the universal approximation property of two-layer neural networks is proved in theory, the achievable numerical accuracy may be far less than the machine precision in practice, for example, when approximating functions with high-frequency components, such as functions with rapid changes or highly oscillatory patterns. Moreover, the numerical errors can not be further improved by increasing the number of data and network width after a certain stage since the number of eigenmodes that can be resolved by a given machine precision does not increase. To deal with these difficulties, one needs to find an appropriate transformation under which the function becomes smooth. On the other hand, the representation is relatively stable to perturbations in the high modes, e.g., noises, or over-parametrization. These phenomena have been well observed and documented in many studies and experiments.

Another key point of using neural networks to represent functions is finding the optimal parameters, a.k.a. learning, as the representation adapts to the underlying function manifested by data. However, we show that the ill-conditioning of the Gram matrix leads to the stiffness of the learning dynamics, which causes long computational time in converging to an accurate approximation of the solution, especially for high-frequency features in the adaptive representation. Moreover, adaptivity may lead to even worse conditioning of the Gram matrix, which causes more stiffness in the dynamics.

From a probabilistic perspective, we show that the Rashomon set, the set of parameters where accurate approximations can be achieved, for two-layer neural networks has a small measure for highly oscillatory functions which decreases exponentially with respect to the oscillation frequency. It implies difficulties in practice, both low probabilities of being close to a good approximation for a random initial guess and higher computational cost for finding one.

All those properties suggest that two-layer neural networks may struggle with high frequencies in practice, even when the universal approximation holds and the optimization process converges theoretically. This has been observed in multiple settings [4, 9, 14]. The authors of [20, 40] argued that such phenomenon should be attributed to the so-called *frequency principle*, that is, the training process of the neural network recovers lower frequencies first. Several explanations based on the frequency principle are proposed. When the activation function $\sigma$ is analytic, e.g., `Tanh` or `Sigmoid`, the authors [40] have shown that the training of the network at the final stage can be slow due to the inability to pick up the high-frequency components. While for non-analytic activation functions e.g., `ReLU`, similar arguments cannot hold due to the non-smoothness. The training process of two-layer `ReLU` neural networks has been studied under a few configurations. Especially the over-parameterized regime [18, 43] and recently the work [13] considered the case that the sample points are not well distributed and zero-initialization for the bias terms.

In this work, we mainly focus on using `ReLU` as the activation function. Our study can be extended to other activation functions as shown in the Appendix. Here is the outline of this paper. First, we present a spectral analysis of the Gram matrix and least square approximation in Section 2. Then we study

the training dynamics based on gradient descent in Section 3. In Section 4, the probability framework and Rashomon set are employed to show why oscillatory functions are difficult to represent and learn. Extension of the current work is briefly discussed in Section 5.

## 2 Gram matrix and least square approximation

We first introduce some notations and the general setup for two-layer neural networks. Denote $[n] = \{1, 2, \cdots, n\}$ and $C(D)$ the continuous functions on a compact domain $D \in \mathbb{R}^d$. Let $\mathcal{H}_n$ be the hypothesis space generated by shallow feed-forward networks of width $n$. Each $h \in \mathcal{H}_n$ has the following form

$$h(\boldsymbol{x}) = \sum_{i=1}^{n} a_i \sigma(\boldsymbol{w}_i \cdot \boldsymbol{x} - b_i) + c \quad \text{for any } \boldsymbol{x} \in \mathbb{R}^d, \tag{1}$$

where $n \in \mathbb{N}^+$ is the width of the network, $\boldsymbol{w}_i \in \mathbb{R}^d$, $a_i, b_i, c \in \mathbb{R}$ are parameters for each $i \in [n]$. Finding the best $h \in \mathcal{H}_n$ to approximate the objective function $f(\boldsymbol{x}) \in C(D)$ is usually converted into minimizing the expected (or true) risk

$$\mathcal{L}(h, f) \coloneqq \mathbb{E}_{\boldsymbol{x} \sim \mathcal{U}(D)} \left[ \ell\big(h(\boldsymbol{x}), f(\boldsymbol{x})\big) \right],$$

where $\mathcal{U}$ is some data distribution over $D$ and $\ell(\cdot, \cdot)$ is a loss function. In practice, only finitely many samples $\big\{ \big(\boldsymbol{x}_i, f(\boldsymbol{x}_i)\big) \big\}_{i=1}^{N}$ are available and the data distribution is unknown. However, one could approximate the expected risk by the empirical risk $\mathcal{L}_{\text{emp}}(h, f)$, which is given by

$$\mathcal{L}_{\text{emp}}(h, f) \coloneqq \frac{1}{N} \sum_{i=1}^{N} \ell\big(h(\boldsymbol{x}_i), f(\boldsymbol{x}_i)\big).$$

In this paper, we let $\mathcal{U}$ be the uniform distribution and $\ell(y, y') = |y - y'|^2$, implying

$$\mathcal{L}(h, f) = \int_D |h(\boldsymbol{x}) - h(\boldsymbol{x})|^2 d\boldsymbol{x} \quad \text{and} \quad \mathcal{L}_{\text{emp}}(h, f) = \frac{1}{N} \sum_{i=1}^{N} |h(\boldsymbol{x}_i) - f(\boldsymbol{x}_i)|^2.$$

A learning/training process is to identify $h^* \in \mathcal{H}_n$ or $\widehat{h} \in \mathcal{H}_n$ such that

$$h^* \in \operatorname*{arg\,min}_{h \in \mathcal{H}_n} \mathcal{L}(h, f) \quad \text{or} \quad \widehat{h} \in \operatorname*{arg\,min}_{h \in \mathcal{H}_n} \mathcal{L}_{\text{emp}}(h, f).$$

This study investigates the approximation capabilities of two-layer neural networks within the mentioned framework. We aim to address the three fundamental questions outlined in the abstract that commonly arise in practical settings.

We start with a study on approximation properties of a two-layer neural network as a linear representation, i.e., where the weights and biases in the hidden neurons are fixed, using least squares. In this setting, the fundamental question is the basis of the representation, i.e., $\{\sigma(\boldsymbol{w}_i \cdot \boldsymbol{x} - b_i), i \in [n]\}$: what space does the basis span and correlation among the basis. Desirable features of a good basis for computational efficiency, accuracy, and stability in practice are sparsity and well-conditioning of the Gram matrix, which is formed by the inner product (or correlation) between each pair of the basis. In other words, global interactions and strong correlations should be avoided.

The most used activation function in neural networks is `ReLU`: $\sigma(x) \coloneqq \max(x, 0)$. The general form of a shallow network in (1) can be simplified to

$$h(\boldsymbol{x}) = \sum_{i=1}^{n} a_i \sigma(\boldsymbol{w}_i \cdot \boldsymbol{x} - b_i) + c, \quad \boldsymbol{x} \in D \subseteq \mathbb{R}^d,\ \boldsymbol{w}_i \in \mathbb{S}^{d-1},\ a_i, b_i \in \mathbb{R}. \tag{2}$$

### 2.1 One-dimensional case

In one dimension, we let $D = [-1, 1]$. Due to the affinity of `ReLU` and the transform $\sigma(x) = x - \sigma(-x)$, the form of a shallow network in (2) can be further simplified to

$$h(x) = c + vx + \sum_{i=1}^{n} a_i \sigma(x - b_i), \quad x \in D,\ c, v, a_i, b_i \in \mathbb{R}.$$

Since we only consider the approximation inside $D$, we may further reduce the network into $h(x) = c + \sum_{i=1}^{n} a_i \sigma(x - b_i)$ by setting $c = f(-1)$ and $b_i \in D$ as well. With fixed $b_i \in D$, ReLU functions $\sigma(x - b_i)$ span the same piecewise linear (in each sub-intervals between $b_i$'s) function space as the finite element basis with nodes $\{b_i\}_{i=1}^n$. Theoretically, they are the same when used in approximating a function in the domain $D$ in the least square setting. The minimizer is the $L_2$ projection of $f(x)$ onto the piecewise linear function space. However, the major difference in practice is the Gram matrix (or normal matrix in linear algebra terminology) of the basis, which defines the linear system one needs to solve numerically to find the best approximation. Using the finite element basis, which is local and well decorrelated, the Gram matrix (or the mass matrix in finite element terminology) is sparse and well-conditioned. The condition number is proportional to the ratio between the sizes of the maximal sub-interval and the minimal sub-interval [16]. While using ReLU functions, which are non-local and can be highly correlated, the Gram matrix is dense and ill-conditioned, as we will show below. As a consequence, 1) computation and memory cost involving the Gram matrix can be very expensive, 2) only those functions close to the linear space spanned by the leading eigenvectors of the Gram matrix can be approximated well. The number of the leading eigenvectors that can be used stably and accurately depends on the decay rate of the eigenvalues, machine precision, and/or noise level. Now we present a spectral analysis of the Gram matrix for a set of ReLU functions.

Denote the Gram matrix $\boldsymbol{G} \coloneqq (\boldsymbol{G}_{i,j}) \in \mathbb{R}^{n \times n}$, where

$$\boldsymbol{G}_{i,j} \coloneqq \int_D \sigma(x - b_i)\sigma(x - b_j)dx = \frac{1}{24}(2 - b_i - b_j - |b_i - b_j|)^2(2 - b_i - b_j + 2|b_i - b_j|).$$

The correlation between two ReLU functions with close biases is $b_i, b_j$ is $1 - O(|b_i - b_j|)$, i.e., highly correlated. To fully understand the spectrum property of $\boldsymbol{G}$, we define the corresponding Gram kernel function $\mathcal{G} : \mathbb{R} \times \mathbb{R} \mapsto \mathbb{R}$:

$$\mathcal{G}(x, y) \coloneqq \int_D \sigma(z - x)\sigma(z - y)dz. \tag{3}$$

In particular, if we restrict $x, y \in D$, then $\mathcal{G}(x, y) = \frac{1}{24}(2 - x - y - |x - y|)^2(2 - x - y + 2|x - y|)$ and its eigenvalues and eigenfunctions can be explicitly computed (see Lemma A.1). The eigenvalues $\mu_k \sim k^{-4}$ and the first few leading eigenfunctions are a combination of exponential functions and Fourier modes, then followed by essentially Fourier modes, from low to high frequencies.

### 2.1.1 Spectral analysis

Denote the vectors $\boldsymbol{a} \coloneqq (a_i)_{i=1}^n$ and $\boldsymbol{f} \coloneqq (f_i)_{i=1}^n$ that $f_i = \int_D f(x)\sigma(x - b_i)dx$. The least-square solution $\boldsymbol{a} \in \mathbb{R}^n$, when the biases are fixed, is $\boldsymbol{a} = \boldsymbol{G}^\dagger \boldsymbol{f}$, where $\boldsymbol{G}^\dagger$ is the pseudo-inverse of $\boldsymbol{G}$. Without loss of generality, we assume that $b_i \neq b_j$ for all $i \neq j$ and the biases are sorted in ascending order, that is, $b_1 < b_2 < \cdots < b_n$. We first provide an estimate for the eigenvalue estimates of the Gram matrix $\boldsymbol{G}$. The rescaled matrix $\boldsymbol{G}_n = \frac{1}{n}\boldsymbol{G}$ is the so-called *kernel matrix* for $\mathcal{G}$, which plays an important role in kernel methods [17]. Proofs of the following results are provided in Appendix A

**Theorem 2.1.** *Suppose $\{b_i\}_{i=1}^n$ are quasi-evenly spaced on $D$, $b_i = -1 + \frac{2(i-1)}{n} + o\left(\frac{1}{n}\right)$. Let $\lambda_1 \geq \lambda_2 \geq \cdots \geq \lambda_n \geq 0$ be the eigenvalues of the Gram matrix $\boldsymbol{G}$, then $|\lambda_k - \frac{n}{2}\mu_k| \leq C$ for some constant $C = \mathcal{O}(1)$, where $\mu_k = \mathcal{O}(k^{-4})$ is the $k$-th eigenvalue of $\mathcal{G}$.*

Generally speaking, if $\{b_i\}_{i=1}^n$ are distributed i.i.d with probability density function $\rho : D \mapsto \mathbb{R}$, then the kernel becomes $\mathcal{G}_\rho(x, y) \coloneqq \rho(x)\mathcal{G}(x, y)\rho(y)$. For this case, we have a similar estimate of eigenvalues if $\rho$ is bounded from below and above by positive constants.

**Corollary 2.2.** *Suppose $b_i$ are i.i.d distributed with probability density function $\rho$ on $D$ such that $0 < \underline{c} \leq \rho(x) \leq \bar{c} < \infty$. Let $\lambda_1 \geq \lambda_2 \geq \cdots \geq \lambda_n \geq 0$ be the eigenvalues of the corresponding Gram matrix $\boldsymbol{G}$, then there is a positive constant $C$ that $|\lambda_k - \frac{n}{2}\mu_k| \leq \frac{Cn}{k^4}\sqrt{\frac{k}{n}\log p^{-1}}$ with probability $1 - p$, where $\mu_k = \mathcal{O}(k^{-4})$ is the $k$-th eigenvalue of $\mathcal{G}_\rho$.*

### 2.1.2 Numerical experiments

Our first two numerical examples show the spectrum of the Gram matrix for ReLU functions in 1D. Figure 1 and the first row of Figure 3 is the plot for eigenvalues in descending order and selected eigenmodes for uniform biases respectively, i.e., $b_j = b_1 + 2(j - 1)/(n - 1)$ for $j \in [n]$ with

$b_1 = -1$. They agree with our analysis perfectly. Figure 2 and the second row of Figure 3 are for non-uniform biases adaptive to the rate of change, i.e., $|f'(x)|$, of $f(x) = \arctan(25x)$ as an example. Define $F(x) = \int_{-1}^{x} |f'(t)|dt / \int_{-1}^{1} |f'(t)|dt$, which is strictly increasing. There exists unique $b_i \in [-1, 1]$ such that $F(b_i) = (i-1)/(n-1)$ for $i \in [n]$. We see that the conditioning becomes a little worse. However, the leading eigenmodes are more adaptive to the rapid change of $f(x)$ at 0. This is demonstrated further when using a least square approximation based on `ReLU` functions with uniform and adaptive biases. In Figure 4, we show the projection of $f$ on the leading eigenmodes corresponding to the Gram matrix. We observe that fewer leading eigenmodes are needed to represent/approximate the target function for adaptive biases compared to uniform biases. Table 1 shows the numerical error in different setups for FEM basis vs. `ReLU` basis (two-layer NN). The final numerical mean square error (MSE), which is directly related to the least square error, is determined by several factors: 1) the grid resolution and the machine precision, which is the same for both; 2) the spectrum of the Gram matrix. When single precision is used in the calculation and $n = 100$ evenly distributed grid points (biases) are used, grid resolution provides the accuracy limit. So the errors for FEM and NN are about the same and the errors are reduced when grids are adaptive to the rapid change of the target function. However, when a very fine grid $n = 1000$ is used, the conditioning of the Gram matrix becomes an important factor. Well-conditioned FEM can reach the machine precision while ill-conditioned NN does not have enough leading eigenmodes (low pass filter) to approximate the target function well and increasing NN width does not help. When double precision is used, even the NN has enough leading eigenmodes to approximate the target function well and the grid resolution becomes the limit for both FEM and NN. Hence the numerical errors for FEM and NN are similar.

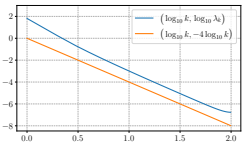

(a) $n = 100$.

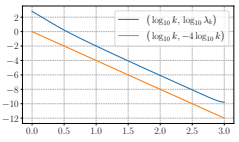

(b) $n = 1000$.

Figure 1: Gram matrix spectrum for uniform $\boldsymbol{b}$.

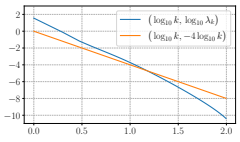

(a) $n = 100$.

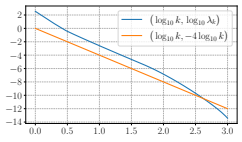

(b) $n = 1000$.

Figure 2: Gram matrix spectrum for adaptive $\boldsymbol{b}$.

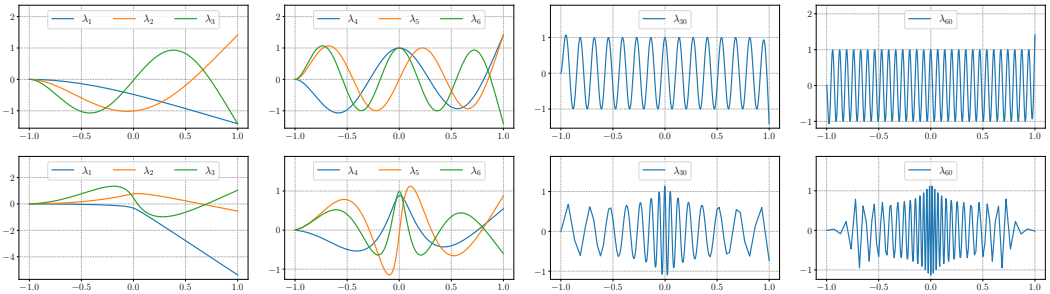

Figure 3: Eigenmodes of $\lambda_k$ for $k = \{1, 2, 3\}, \{4, 5, 6\}, 30, 60$ with $n = 1000$. The first and second rows correspond to uniform and adaptive $\boldsymbol{b}$, respectively.

Table 1: Error comparison for approximating $f(x) = \arctan(25x)$ with sufficient samples.

| | | float32 | | | | float64 | | | |
|---|---|---|---|---|---|---|---|---|---|
| | | $n = 100$ | | $n = 1000$ | | $n = 100$ | | $n = 1000$ | |
| | | MAX | MSE | MAX | MSE | MAX | MSE | MAX | MSE |
| NN | Uniform $\boldsymbol{b}$ | $6.09 \times 10^{-2}$ | $9.58 \times 10^{-5}$ | $7.19 \times 10^{-2}$ | $1.43 \times 10^{-4}$ | $1.37 \times 10^{-2}$ | $1.70 \times 10^{-6}$ | $1.05 \times 10^{-4}$ | $1.33 \times 10^{-10}$ |
| FEM | Uniform $\boldsymbol{b}$ | $1.37 \times 10^{-2}$ | $1.70 \times 10^{-6}$ | $1.05 \times 10^{-4}$ | $1.33 \times 10^{-10}$ | $1.37 \times 10^{-2}$ | $1.70 \times 10^{-6}$ | $1.05 \times 10^{-4}$ | $1.33 \times 10^{-10}$ |
| NN | Adaptive $\boldsymbol{b}$ | $6.83 \times 10^{-2}$ | $7.54 \times 10^{-5}$ | $1.89 \times 10^{-2}$ | $1.06 \times 10^{-5}$ | $3.93 \times 10^{-3}$ | $1.42 \times 10^{-6}$ | $4.74 \times 10^{-5}$ | $1.17 \times 10^{-10}$ |
| FEM | Adaptive $\boldsymbol{b}$ | $2.92 \times 10^{-3}$ | $9.95 \times 10^{-7}$ | $3.79 \times 10^{-5}$ | $1.02 \times 10^{-10}$ | $2.92 \times 10^{-3}$ | $9.95 \times 10^{-7}$ | $3.77 \times 10^{-5}$ | $1.02 \times 10^{-10}$ |

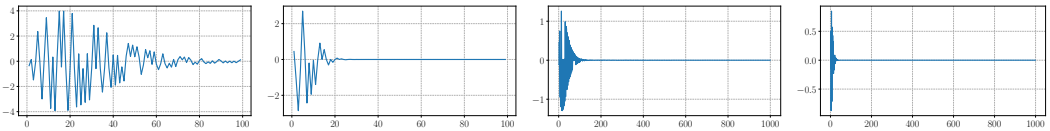

(a) Uniform $\boldsymbol{b}$, $n = 100$. (b) Adaptive $\boldsymbol{b}$, $n = 100$. (c) Uniform $\boldsymbol{b}$, $n = 1000$. (d) Adaptive $\boldsymbol{b}$, $n = 1000$.

Figure 4: Projection of $f$ on the eigenmodes of the Gram matrix: coefficients vs. eigenmode index.

In the following experiment, we show the low-pass filter nature of two-layer neural networks (NN) vs. finite element (FEM) basis with respect to noise and overfitting (or over-parametrization). The target function is $f(x) = \cos(3\pi x) - \sin(\pi x)$ with noise sampled from $\mathcal{U}(-0.5, 0.5)$ in our test. We manually select the cut-off ratio, $\eta$ [2] for small singular values. The numerical results are shown in Figure 5 and Table 2 for evenly distributed $b_i$. Since FEM has a condition number of $\mathcal{O}(1)$, all modes resolved by the grid are captured independent of the cut-off ratio $\eta$. On the other hand, NN only captures the leading eigenmodes, the number of which is determined by $\eta$. We can see that NN captures more modes as $\eta$ becomes smaller (less regularized). It is also interesting to see the low pass filter effect when the Adam optimizer is used to minimize the least square, which is related to the learning dynamics analysis in Section 3. In the case of 1000 data points and 1500 degrees of freedom, Figure 6 shows that a two-layer `ReLU` network is significantly more stable with respect to over-parametrization due to its low-pass filter nature.

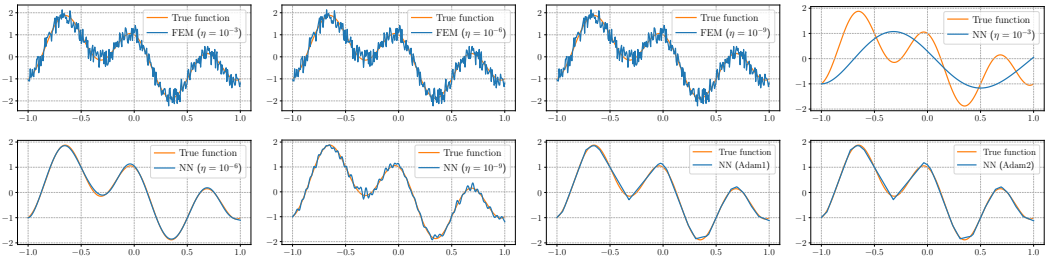


Figure 5: Approximation stability: FEM vs. NN subject to uniform noise $\mathcal{U}(-0.5, 0.5)$ on 1000 samples and $n = 1000$ basis. The first six plots are results from the least square with different cut-off ratio $\eta$ for singular values. The last two plots are the results trained by the Adam optimizer, where "Adam1" and "Adam2" use single and double precision, respectively.

Table 2: Approximation errors in Figure 5.

| | least square | | | | | | Adam optimizer | |
|---|---|---|---|---|---|---|---|---|
| | FEM ($\eta = 10^{-3}$) | FEM ($\eta = 10^{-6}$) | FEM ($\eta = 10^{-9}$) | NN ($\eta = 10^{-3}$) | NN ($\eta = 10^{-6}$) | NN ($\eta = 10^{-9}$) | NN (float32) | NN (float64) |
| maximum error | $4.98 \times 10^{-1}$ | $4.98 \times 10^{-1}$ | $4.98 \times 10^{-1}$ | 1.80 | $1.01 \times 10^{-1}$ | $3.28 \times 10^{-1}$ | $1.43 \times 10^{-1}$ | $1.39 \times 10^{-1}$ |
| mean square error | $5.63 \times 10^{-2}$ | $5.63 \times 10^{-2}$ | $5.63 \times 10^{-2}$ | $7.60 \times 10^{-1}$ | $1.34 \times 10^{-3}$ | $7.03 \times 10^{-3}$ | $2.74 \times 10^{-3}$ | $2.76 \times 10^{-3}$ |

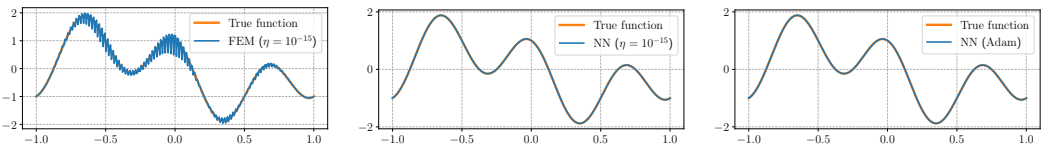


Figure 6: Test of overfitting: FEM vs. NN with 1000 samples, $n = 1500$ basis, and double precision. The first two plots are results from least square, where $\eta$ is the cut-off ratio for small singular values. The last plot is the result trained by the Adam optimizer.

### 2.2 Multi-dimensional case

Now we provide the spectral analysis for `ReLU` functions in arbitrary dimensions, although we cannot compute the eigenvalues and eigenfunctions explicitly. In this section, we consider domain

[2] Singular values are treated as zero if they are smaller than $\eta$ times the largest singular value.

$D = B_d(1)$ which is the unit ball in $d$-dimension. The class of neural network $\mathcal{H}$ is

$$h(x) = c + \sum_{i=1}^{n} a_i \sigma(\boldsymbol{w}_i \cdot \boldsymbol{x} - b_i) \quad \boldsymbol{w}_i \in \mathbb{S}^{d-1},\ b_i \in [-1, 1].$$

We set $c = f(\mathbf{0})$ for simplicity. Similar to the 1D setting, we consider the corresponding continuous kernel $\mathcal{G} : L^2(\mathbb{S}^{d-1} \times [-1, 1]) \mapsto L^2(\mathbb{S}^{d-1} \times [-1, 1])$

$$\mathcal{G}(\boldsymbol{w}, b, \boldsymbol{w}', b') = \int_D \sigma(\boldsymbol{w} \cdot \boldsymbol{x} - b)\sigma(\boldsymbol{w}' \cdot \boldsymbol{x} - b')d\boldsymbol{x} \quad \boldsymbol{w}, \boldsymbol{w}' \in \mathbb{S}^{d-1},\ b, b' \in [-1, 1].$$

Let $(\lambda_k, \phi_k)$ be the $k$-th eigenpair which satisfies

$$\int_{\mathbb{S}^{d-1}\times[-1,1]} \mathcal{G}(\boldsymbol{w}, b, \boldsymbol{w}', b')\phi_k(\boldsymbol{w}', b')d\boldsymbol{w}'db' = \lambda_k \phi_k(\boldsymbol{w}, b).$$

We show the following eigenvalue estimate and for more general cases (Remark B.5) in Appendix B.

**Theorem 2.3.** *There are constants $c_1, c_2 > 0$, depending on $D$ and $d$, such that $c_1 k^{-(d+3)/d} \leq \lambda_k \leq c_2 k^{-(d+3)/d}$, ($\lambda_k = \Theta(k^{-(d+3)/d})$ using Landau notation).*

The spectrum of the discrete Gram matrix has a similar behavior when $\boldsymbol{w}_i \in \mathbb{S}^{d-1},\ b_i \in [-1, 1]$ are uniformly distributed as shown in the following 2D experiment. We use 25600 evenly spaced samples for $(\boldsymbol{w}, b) \in \mathbb{S}^1 \times [-1, 1]$. The spectrum of the Gram matrix is shown in Figure 7. We present several eigenmodes in Figure 8. In practice, those high-frequency modes are difficult to capture when the corresponding eigenvalues are smaller than machine precision.

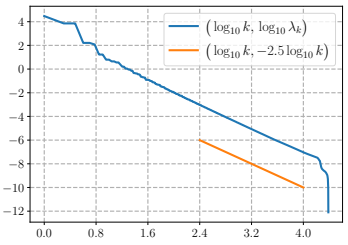


Figure 7: 2D spectrum.

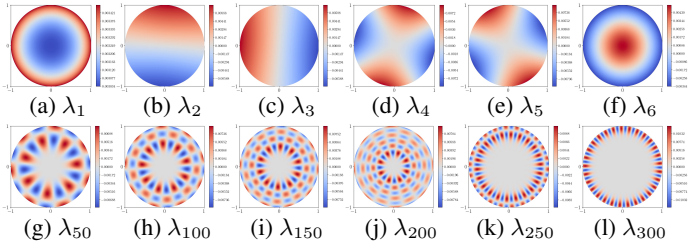


Figure 8: Eigenmodes of $\lambda_k$ with $n = 25600$.

**Remark 2.4.** *Although the decay of eigenvalues seems slower in higher dimensions, however, the number of Fourier modes less than frequency $\nu$ is $\Theta(\nu^d)$. In other words, given a machine precision $\varepsilon$, no matter how wide a two-layer neural network is, it can resolve all Fourier modes up to frequency $\mathcal{O}(\varepsilon^{-\frac{1}{d+3}})$. In practice, the ill-conditioning of the Gram matrix may be less severe in higher dimensions since the dense sampling of $\boldsymbol{w}_i$ and $b_i$ may not be affordable.*

### 2.3 Some comments

Based on the above analysis and numerical experiments, we give a few comments on using shallow neural networks, many of which have been well observed in practice.

**Low-pass filter nature**. For evenly or uniformly distributed bounded weights and biases, given a fixed machine precision, $\varepsilon$, no matter how wide a two-layer neural network is, it can stably resolve at most $\mathcal{O}(\varepsilon^{-\frac{d}{d+3}})$ leading eigenmodes of the Gram matrix in $d$-dimensions. This is because, after reaching a certain sampling density, the eigenvalues and eigenfunctions are very close to those of the continuous kernel. In practice, $\boldsymbol{G}^{-1}$ is typically approximated/regularized by its Moore-Penrose pseudo-inverse $\boldsymbol{G}^{\dagger}$ by cutting off the small eigenvalues at a threshold of $n\varepsilon\lambda_1$, where $n$ is the matrix size and $\varepsilon$ is the machine precision. The machine precision for single and double precision are: $\varepsilon_1 = 2^{-23}$ and $\varepsilon_2 = 2^{-52}$ respectively. Hence, a two-layer neural network can resolve about $2^{23d/(d+3)}$ and $2^{52d/(d+3)}$ eigenmodes respectively in $d$-dimensions. Since the leading eigenmodes are the smoother ones, the resulting approximation behaves like a low-pass filter. The number of modes in each direction that can be resolved is $2^{23/(d+3)}$ and $2^{52/(d+3)}$ respectively in $d$-dimensions, which is roughly $54\ (d = 1), 25\ (d = 2), 14\ (d = 3)$, and $4\ (d = 10)$ for single precision, and $8192\ (d = 1), 1351\ (d = 2), 411\ (d = 3)$, and $16\ (d = 10)$ for double precision.

**Implications**. The low-pass filter nature explains why it is widely observed that shallow neural networks can approximate smooth function well. In practice, one can obtain a numerical error close to machine precision. On the other hand, for functions with sharp transitions or rapid oscillations, one may acquire a certain numerical error that is far from machine precision even using *wide* shallow networks for which universal approximation is proved in theory. The low-pass filter nature of the shallow neuron networks also implies stability with respect to noises or overfitting/over-parametrization.

To approximate a more complicated target function well, one needs to design an appropriate transformation or change of variables under which the target function becomes smooth and hence can be approximated well by a two-layer neural network.

## 3 Learning dynamics

The key feature in machine learning using neural network representation is the training process, which ideally can find the optimal parameters, i.e., an adaptive representation driven by the data. The relevant approximation theory has been studied extensively. The best-known approximation error estimates using `ReLU` as the activation function for two-layer neural network [2, 23] are based on the fact that $\sigma''(t) = \delta(t)$, which implies $\Delta f$ can be expressed as a standard Radon transform when viewing the parameters $\{a_i\}_{i=1}^n$ as an empirical measure of $(\boldsymbol{w}, b) \in \mathbb{S}^{d-1} \times \mathbb{R}$. In practice, gradient-based methods (and the variants) are adopted to seek the optimal parameters. Here we study the following natural question: assuming that a gradient-based optimization can find the optimal solution, which itself is a challenging question in general, what are the training dynamics and its computation cost to attain such a solution from a random initial guess?

Our previous analysis shows that a two-layer neural network with fixed (or randomly sampled) biases will have a low-pass filter nature under finite machine precision, which makes it challenging to capture high-frequency components, i.e., fine-scale features. Here we show that the ill-conditioning of the Gram matrix causes difficulties in the learning process as well. In particular, we demonstrate that initial high-frequency component error can take a long time to correct. All these lead to numerical difficulties in achieving the optimal solution even if one assumes the learning process can find the optimal solution in theory. It implies that even if the complete learning process is applied, the numerical error can still be far from the machine precision for functions with high-frequency components in practice.

Training a neural network with the gradient flow can be regarded as the gradient descent method with a very small step size for finite time dynamics. We use 1D as an example. Let $D = [-1, 1]$, the gradient flow of $\{a_i\}_{i=1}^n$ and $\{b_i\}_{i=1}^n$ follow

$$\frac{da_i}{dt} = -\int_D (h(x,t) - f(x))\sigma(x - b_i)dx \quad \text{and} \quad \frac{db_i}{dt} = a_i \int_D (h(x,t) - f(x))\sigma'(x - b_i)dx.$$

One popular way to analyze the dynamics of the neuron network is the mean-field representation and the network is written as

$$\overline{h}(x,t) = \int_{\mathbb{R}^2} a\sigma(x - b)\mu_n(a, b, t)dadb$$

with empirical measure $\mu_n(a, b, t) = \frac{1}{n}\sum_{i=1}^n \delta(a - a_i(t), b - b_i(t))$. The analysis of the limiting behavior of mean-field neural networks can be found in [21, 26, 35] and the references therein. However, most of the mean-field studies assume the measure $\mu_n(\cdot, \cdot, t)$ converges as $t \to \infty$ and $n \to \infty$.

Our study works for fully discrete two-layer neural networks with no convergence assumption for the measure $\mu_n$ or requiring $n \to \infty$. The main difficulty for our analysis is the possibility of biases $b_i$ moving out of the bounded domain of interest. Define generalized Fourier modes, $\{\theta_m\}_{m\geq 1}$, which are the eigenfunctions of the Gram kernel $\mathcal{G}$ in (3), and $\widehat{g}$ as the generalized discrete Fourier transform of $g$,

$$\widehat{g}(m) = \int_D g(x)\theta_m(x)dx.$$

In 1D, the generalized Fourier transform is close to the standard Fourier transform for high modes. The key to our study is the construction of an auxiliary function (defined by (11) in Appendix C)

$w(x,t) \in C^2(D)$ that satisfies $\partial_x^2 w(x,t) = h(x,t) - f(x) = e(x,t)$, which is the approximating error at time $t$, with boundary conditions $w(1,t) = \partial_x w(1,t) = 0$. By studying the evolution of $\widehat{w}(m,t)$ we show at least how slow the learning dynamics can be in terms of the lower bound for time needed to reduce the initial error in mode $m$. Under the following mild assumptions: 1) There exists a constant $M > 0$ that $\sup_{i=1}^n |a_i(t)|^2 \leq M$; 2) The initialization of biases $\{b_i(0)\}_{i=1}^n$ are equispaced on $D$, We prove (see Appendix C)

**Theorem 3.1.** *If $|\widehat{w}(m,0)| \neq 0$, then it will take at least $\mathcal{O}(\frac{m^3|\widehat{w}(m,0)|}{n})$ time to reduce the generalized Fourier coefficient by half, i.e., $|\widehat{w}(m,t)| \leq \frac{1}{2}|\widehat{w}(m,0)|$.*

In numerical computation, to follow the gradient flow closely, the discrete time-step is $\mathcal{O}(\frac{1}{n})$. From the relation $|\widehat{w}(m,t)| \simeq m^{-2}|\widehat{e}(m,t)|$, Theorem 3.1 says that if the initial error in mode $m$, $|\widehat{e}(m,0)| \neq 0$, (which means $|\widehat{w}(m,0)| > cm^{-2}$ for some $c > 0$,) it takes at least $\mathcal{O}(m)$ steps to reduce the error in mode $m$ by half. Note that the result does not depend on the convergence of the optimization algorithm and the above estimate is a lower bound. In practice, the gradient-based training process could have an even slower learning rate. In the next theorem, the lower bound is improved in a more specific scaling regime (in terms of network width vs. frequency mode) and using a better estimate (see Appendix C). It implies that it takes at least $\mathcal{O}(m^2)$ steps to reduce the error in mode $m$ by half in numerical computation. In the special case of fixed biases (i.e., least square problem), the number of steps needed is $\mathcal{O}(m^3)$ (see Remark C.18)

**Theorem 3.2.** *If the total variation of the sequence $\{a_i^2(t)\}_{i=1}^n$ is bounded by $M'$. Let $n \geq m^4$ be sufficiently large, then it will take at least $\mathcal{O}(\frac{m^4|\widehat{w}(m,0)|}{n})$ time to reduce the generalized Fourier coefficient by half, i.e., $|\widehat{w}(m,t)| \leq \frac{1}{2}|\widehat{w}(m,0)|$.*

The above results show that reducing the initial error in high-frequency modes by gradient-based learning dynamics is slow. Moreover, due to the low-pass filter nature shown earlier, it is difficult to capture high-frequency modes for two-layer neural networks with evenly or uniformly distributed initial biases. Due to these two effects it shows why a two layer neural network struggles with high-frequency modes in approximation even if a full training process is employed.

## 4 Rashomon set for two-layer ReLU neural networks

In [28, 29], the authors claimed that the measure of the so-called Rashomon set can be used as a criterion to see if a simple model exists for the approximation problem. Let $D = B_d(1)$ be the unit ball in $\mathbb{R}^d$. The Rashomon set $\mathcal{R}_\varepsilon \subseteq \mathbb{R}^m$ for the two-layer neural network class $\mathcal{H}_n$ is defined as the following

$$\mathcal{R}_\varepsilon := \{h \in \mathcal{H}_n \mid \|h - f\|_{L^2(D)} \leq \varepsilon \|f\|_{L^2(D)}\},$$

where $m$ is the number of parameters for $\mathcal{H}_n$. If we normalize the measure for $\mathcal{H}_n$, the measure of the Rashomon set quantifies the probability that the loss is under a certain threshold for a random pick of parameters. The main purpose of this section is to characterize the probability measure of the Rashomon set with $\mathcal{H}_n$ representing the two-layer `ReLU` neural networks

$$h(\boldsymbol{x}) = \frac{1}{n}\sum_{j=1}^n a_j \sigma(\boldsymbol{w}_j \cdot \boldsymbol{x} - b_j) + \boldsymbol{v} \cdot \boldsymbol{x} + c, \quad \boldsymbol{x} \in D \subseteq \mathbb{R}^d.$$

where the parameters $\{a_j\}_{j=1}^n$ are bounded by $[-A, A]$ and $\{b_i\}_{i=1}^n \subseteq [-1, 1]$. It is already known that this network can approximate an admissible function with an error no more than $\mathcal{O}(\sqrt{d + \log n}\, n^{-1/2-1/d})$ [2]. Taking Laplacian on $h$,

$$\Delta h(\boldsymbol{x}) = \frac{1}{n}\sum_{j=1}^n a_j \Delta\sigma(\boldsymbol{w}_j \cdot \boldsymbol{x} - b_j) = \frac{1}{n}\sum_{j=1}^n a_j \delta(\boldsymbol{w}_j \cdot \boldsymbol{x} - b_j).$$

**Theorem 4.1.** *Suppose $f \in C(D)$ such that there exists $g \in C_0^2(D)$ that $\Delta g = f$, then the Rashomon set $\mathcal{R}_\varepsilon \subseteq \mathcal{H}$ satisfies*

$$\mathbb{P}(\mathcal{R}_\varepsilon) \leq \exp\left(-\frac{n(1-\varepsilon)^2\|f\|_{L^2(D)}^4}{2A^2\kappa^2}\right), \quad \kappa := \sup_{(\boldsymbol{w},b)} \int_{\{\boldsymbol{x}\in D, \boldsymbol{w}\cdot\boldsymbol{x}=b\}} g(\boldsymbol{x}) dH_{d-1}(\boldsymbol{x}).$$

If $f$ oscillates with frequency $\nu$ in every direction, then $\kappa \approx \nu^{-2}$ and the probability measure of Rashomon set scales as $\exp(-\mathcal{O}(\nu^{-4}))$ which gives another perspective why oscillatory functions are difficult to approximate by neural networks in general. The proof and extension to more general activation functions are provided in Appendix D.2.

## 5 Further discussions

In this study, it is shown that the use of highly correlated activation functions in a two-layer neural network makes it filter out fine features (high-frequency components) when finite machine precision is imposed, which is an implicit regularization in practice. Moreover, increasing the network width does not improve the numerical accuracy after a certain threshold is reached, although the universal approximation property is proved in theory. The smoother the activation function is, the faster the Gram matrix spectrum decays (see Remark B.5 and Appendix E), and hence the stronger the regularization is. Similar studies for deep neural networks will be both interesting and challenging.


## Acknowledgments and Disclosure of Funding

H. Zhao was partially supported by NSF grants DMS-2309551, and DMS-2012860. Y. Zhong was partially supported by NSF grant DMS-2309530, H. Zhou was partially supported by NSF grant DMS-2307465.


## References


[1] Chenglong Bao, Qianxiao Li, Zuowei Shen, Cheng Tai, Lei Wu, and Xueshuang Xiang. Approximation analysis of convolutional neural networks. *Semantic Scholar e-Preprint*, page Corpus ID: 204762668, 2019.

[2] Andrew R. Barron and Jason M. Klusowski. Approximation and estimation for high-dimensional deep learning networks. *arXiv e-prints*, page arXiv:1809.03090, September 2018.

[3] Johan M Bogoya, Albrecht Böttcher, and Alexander Poznyak. Eigenvalues of hermitian toeplitz matrices with polynomially increasing entries. *Journal of Spectral Theory*, 2(3):267–292, 2012.

[4] Jingrun Chen, Xurong Chi, Zhouwang Yang, et al. Bridging traditional and machine learning-based algorithms for solving pdes: The random feature method. *arXiv preprint arXiv:2207.13380*, 2022.

[5] Minshuo Chen, Haoming Jiang, Wenjing Liao, and Tuo Zhao. Efficient approximation of deep ReLU networks for functions on low dimensional manifolds. In H. Wallach, H. Larochelle, A. Beygelzimer, F. d'Alché-Buc, E. Fox, and R. Garnett, editors, *Advances in Neural Information Processing Systems*, volume 32. Curran Associates, Inc., 2019.

[6] Charles K. Chui, Shao-Bo Lin, and Ding-Xuan Zhou. Construction of neural networks for realization of localized deep learning. *Frontiers in Applied Mathematics and Statistics*, 4:14, 2018.

[7] Georg Frobenius. Über matrizen aus nicht negativen elementen. *Sitzungsberichte der Königlich Preussischen Akademie der Wissenschaften*, 23:456–477, 1912.

[8] Rémi Gribonval, Gitta Kutyniok, Morten Nielsen, and Felix Voigtlaender. Approximation spaces of deep neural networks. *Constructive Approximation*, 55:259–367, 2022.

[9] Tamara G Grossmann, Urszula Julia Komorowska, Jonas Latz, and Carola-Bibiane Schönlieb. Can physics-informed neural networks beat the finite element method? *arXiv preprint arXiv:2302.04107*, 2023.

[10] Ingo Gühring, Gitta Kutyniok, and Philipp Petersen. Error bounds for approximations with deep ReLU neural networks in $W^{s,p}$ norms. *Analysis and Applications*, 18(05):803–859, 2020.

[11] Sigurdur Helgason. *Groups and geometric analysis: integral geometry, invariant differential operators, and spherical functions*, volume 83. American Mathematical Society, 2022.

[12] Sigurdur Helgason et al. *Integral geometry and Radon transforms*. Springer, 2011.

[13] David Holzmüller and Ingo Steinwart. Training two-layer relu networks with gradient descent is inconsistent. *arXiv preprint arXiv:2002.04861*, 2020.

[14] Qingguo Hong, Qinyang Tan, Jonathan W Siegel, and Jinchao Xu. On the activation function dependence of the spectral bias of neural networks. *arXiv preprint arXiv:2208.04924*, 2022.

[15] Yuling Jiao, Yanming Lai, Xiliang Lu, Fengru Wang, Jerry Zhijian Yang, and Yuanyuan Yang. Deep neural networks with ReLU-Sine-Exponential activations break curse of dimensionality on hölder class. *arXiv e-prints*, page arXiv:2103.00542, February 2021.

[16] Lennard Kamenski, Weizhang Huang, and Hongguo Xu. Conditioning of finite element equations with arbitrary anisotropic meshes. *Mathematics of Computation*, 83(289):2187–2211, 2014.

[17] Vladimir Koltchinskii and Evarist Giné. Random matrix approximation of spectra of integral operators. *Bernoulli*, 6(1):113–167, 2000.

[18] Yuanzhi Li, Tengyu Ma, and Hongyang R Zhang. Learning over-parametrized two-layer relu neural networks beyond ntk. *arXiv preprint arXiv:2007.04596*, 2020.

[19] Jianfeng Lu, Zuowei Shen, Haizhao Yang, and Shijun Zhang. Deep network approximation for smooth functions. *SIAM Journal on Mathematical Analysis*, 53(5):5465–5506, 2021.

[20] Tao Luo, Zheng Ma, Zhi-Qin John Xu, and Yaoyu Zhang. Theory of the frequency principle for general deep neural networks. *arXiv preprint arXiv:1906.09235*, 2019.

[21] Song Mei, Andrea Montanari, and Phan-Minh Nguyen. A mean field view of the landscape of two-layer neural networks. *Proceedings of the National Academy of Sciences*, 115(33):E7665–E7671, 2018.

[22] Ryumei Nakada and Masaaki Imaizumi. Adaptive approximation and generalization of deep neural network with intrinsic dimensionality. *Journal of Machine Learning Research*, 21(174):1–38, 2020.

[23] Greg Ongie, Rebecca Willett, Daniel Soudry, and Nathan Srebro. A function space view of bounded norm infinite width relu nets: The multivariate case. *arXiv preprint arXiv:1910.01635*, 2019.

[24] JB Reade. Eigenvalues of positive definite kernels. *SIAM Journal on Mathematical Analysis*, 14(1):152–157, 1983.

[25] JB Reade. Eigenvalues of positive definite kernels ii. *SIAM journal on mathematical analysis*, 15(1):137–142, 1984.

[26] Grant M Rotskoff and Eric Vanden-Eijnden. Trainability and accuracy of neural networks: An interacting particle system approach. *arXiv preprint arXiv:1805.00915*, 2018.

[27] Pedro Savarese, Itay Evron, Daniel Soudry, and Nathan Srebro. How do infinite width bounded norm networks look in function space? In *Conference on Learning Theory*, pages 2667–2690. PMLR, 2019.

[28] Lesia Semenova, Cynthia Rudin, and Ronald Parr. A study in rashomon curves and volumes: A new perspective on generalization and model simplicity in machine learning. *arXiv preprint arXiv:1908.01755*, 2019.

[29] Lesia Semenova, Cynthia Rudin, and Ronald Parr. On the existence of simpler machine learning models. In *2022 ACM Conference on Fairness, Accountability, and Transparency*, pages 1827–1858, 2022.

[30] Zuowei Shen, Haizhao Yang, and Shijun Zhang. Nonlinear approximation via compositions. *Neural Networks*, 119:74–84, 2019.

[31] Zuowei Shen, Haizhao Yang, and Shijun Zhang. Deep network approximation characterized by number of neurons. *Communications in Computational Physics*, 28(5):1768–1811, 2020.

[32] Zuowei Shen, Haizhao Yang, and Shijun Zhang. Deep network with approximation error being reciprocal of width to power of square root of depth. *Neural Computation*, 33(4):1005–1036, 03 2021.

[33] Zuowei Shen, Haizhao Yang, and Shijun Zhang. Neural network approximation: Three hidden layers are enough. *Neural Networks*, 141:160–173, 2021.

[34] Zuowei Shen, Haizhao Yang, and Shijun Zhang. Deep network approximation: Achieving arbitrary accuracy with fixed number of neurons. *Journal of Machine Learning Research*, 23(276):1–60, 2022.

[35] Justin Sirignano and Konstantinos Spiliopoulos. Mean field analysis of neural networks: A central limit theorem. *Stochastic Processes and their Applications*, 130(3):1820–1852, 2020.

[36] Taiji Suzuki. Adaptivity of deep ReLU network for learning in Besov and mixed smooth Besov spaces: optimal rate and curse of dimensionality. In *International Conference on Learning Representations*, 2019.

[37] Ernesto Araya Valdivia. Relative concentration bounds for the spectrum of kernel matrices. *arXiv preprint arXiv:1812.02108*, 2018.

[38] Roman Vershynin. *High-dimensional probability: An introduction with applications in data science*, volume 47. Cambridge university press, 2018.

[39] Harold Widom. On the eigenvalues of certain hermitian operators. *Transactions of the American Mathematical Society*, 88(2):491–522, 1958.

[40] Zhi-Qin John Xu, Yaoyu Zhang, Tao Luo, Yanyang Xiao, and Zheng Ma. Frequency principle: Fourier analysis sheds light on deep neural networks. *arXiv preprint arXiv:1901.06523*, 2019.

[41] Dmitry Yarotsky. Error bounds for approximations with deep ReLU networks. *Neural Networks*, 94:103–114, 2017.

[42] Dmitry Yarotsky. Optimal approximation of continuous functions by very deep ReLU networks. In Sébastien Bubeck, Vianney Perchet, and Philippe Rigollet, editors, *Proceedings of the 31st Conference On Learning Theory*, volume 75 of *Proceedings of Machine Learning Research*, pages 639–649. PMLR, 06–09 Jul 2018.

[43] Guodong Zhang, James Martens, and Roger B Grosse. Fast convergence of natural gradient descent for over-parameterized neural networks. *Advances in Neural Information Processing Systems*, 32, 2019.

[44] Shijun Zhang. Deep neural network approximation via function compositions. *PhD Thesis, National University of Singapore*, 2020. URL: https://scholarbank.nus.edu.sg/handle/10635/186064.

[45] Shijun Zhang, Jianfeng Lu, and Hongkai Zhao. On Enhancing Expressive Power via Compositions of Single Fixed-Size ReLU Network. *arXiv e-prints*, page arXiv:2301.12353, January 2023.

[46] Shijun Zhang, Zuowei Shen, and Haizhao Yang. Neural network architecture beyond width and depth. In S. Koyejo, S. Mohamed, A. Agarwal, D. Belgrave, K. Cho, and A. Oh, editors, *Advances in Neural Information Processing Systems*, volume 35, pages 5669–5681. Curran Associates, Inc., 2022.

[47] Ding-Xuan Zhou. Universality of deep convolutional neural networks. *Applied and Computational Harmonic Analysis*, 48(2):787–794, 2020.

## Contents of main article and appendix

## A Eigenvalues of Gram matrix in one dimension

**Lemma A.1.** *Define the Gram kernel function*

$$\begin{aligned}\mathcal{G}(x,y) &\coloneqq \frac{1}{24}(2-x-y-|x-y|)^2(2-x-y+2|x-y|)\\ &= \frac{1}{12}|x-y|^3+\frac{1}{12}(2-x-y)\left(2(1-x)(1-y)-(x-y)^2\right).\end{aligned}$$

*and let operator* $K: L^2[-1,1]\to L^2[-1,1]$

$$Kh(x)=\int_{-1}^{1}\mathcal{G}(x,y)h(y)dy,$$

*and denote* $\mu_j$ *is the* $j$*-th eigenvalue of* $K$ *in descending order, then there exist positive constants* $c_1$ *and* $c_2$ *that* $c_1 j^{-4}\le\mu_j\le c_2 j^{-4}$.

*Proof.* Assume the eigenpairs of $K$ are denoted by $(\mu_k,\psi_k)$, $k\ge 1$, where $\mu_k$ are sorted in descending order. For the eigenfunction $\psi_k$, it satisfies

$$\int_{-1}^{1}\mathcal{G}(x,y)\psi_k(y)dy=\mu_k\psi_k(x), \tag{4}$$

Taking derivatives four times on both sides, similar techniques can be found in [3], we obtain the following differential equation,

$$\psi^{(4)}(x)=\frac{1}{\mu_k}\psi_k(x).$$

which implies that there are constants $A_s\in\mathbb{C}$, $0\le s\le 3$ that

$$\psi_k(x)=A_0\cosh(w_kx)+A_1\sinh(w_kx)+A_2\cos(w_kx)+A_3\sin(w_kx)$$

for certain $w_k=\mu_k^{-\frac{1}{4}}>0$. Thus solving the eigensystem is then equivalent to solving a $4\times 4$ matrix $P$ that $\det(P)=0$ for $\omega$ using (4). Observe that $\mathcal{G}(1,y)=0$, $\mathcal{G}_x(1,y)=0$, $\mathcal{G}_{xx}(1,y)=1-y$ and $\mathcal{G}_{xxx}(1,y)=1$. We find the corresponding equation as

$$\begin{pmatrix}\cosh(w_k) & \sinh(w_k) & \cos(w_k) & \sin(w_k)\\ w_k\sinh(w_k) & w_k\cosh(w_k) & -w_k\sin(w_k) & w_k\cos(w_k)\\ w_k^2\cosh(w_k) & w_k^2\sinh(w_k) & -w_k^2\cos(w_k) & -w_k^2\sin(w_k)\\ w_k^3\sinh(w_k) & w_k^3\cosh(w_k) & w_k^3\sin(w_k) & -w_k^3\cos(w_k)\end{pmatrix}\begin{pmatrix}A_0\\A_1\\A_2\\A_3\end{pmatrix}$$

$$=w_k^4\begin{pmatrix}0\\0\\\frac{2\sinh(w_k)}{w_k}A_0+\frac{2\sinh(w_k)-2\cosh(w_k)}{w_k^2}A_1+\frac{2\sin(w_k)}{w_k}A_2+\frac{2w_k\cos(w_k)-2\sin(w_k)}{w_k^2}A_3\\ \frac{2\sinh(w_k)}{w_k}A_0+\frac{2\sin(w_k)}{w_k}A_2\end{pmatrix}.$$

Let the determinant of the above linear equation be zero which gives the following simple relation

$$\tan(w_k)\tanh(w_k)=\pm 1.$$

Let $g(x)=\tan(x)\tanh(x)$, for $x\in(n\pi,n\pi+\frac{\pi}{2})$ or $x\in(n\pi+\frac{\pi}{2},n\pi+\frac{3\pi}{2})$, $n\in\mathbb{Z}$, the function $g$ is monotone and has a range of $(-\infty,\infty)$ in each interval. Therefore there is a unique $w_{2j+1}\in((j+\frac{1}{4})\pi,(j+\frac{1}{2})\pi)$, $w_{2j+2}\in((j+\frac{1}{2})\pi,(j+\frac{3}{4})\pi)$, $j\ge 0$, which says $\lambda_j\sim(\frac{j}{2}\pi)^{-4}$. Actually, one can show that both $c_1=\left(\frac{2}{\pi}\right)^4(1+\mathcal{O}(j^{-1}))$ and $c_2=\left(\frac{2}{\pi}\right)^4(1+\mathcal{O}(j^{-1}))$. Moreover, we can derive the explicit forms for the eigenfunctions:

1. If $\tan(w_k)\tanh(w_k)=1$, $\psi_k(x)=A_2(-\frac{\cos(w_k)}{\sinh(w_k)}\sinh(w_kx)+\cos(w_kx))$,
2. If $\tan(w_k)\tanh(w_k)=-1$, $\psi_k(x)=A_3(-\frac{\sin(w_k)}{\cosh(w_k)}\cosh(w_kx)+\sin(w_kx))$.

One can observe that $A_0,A_1=\mathcal{O}(e^{-w_k})$. A quick computation of normalization shows that $A_2,A_3$ are uniformly bounded, which implies that all eigenfunctions are uniformly bounded. □

In fact, one can derive a much more accurate estimate of $w_k$, $k \in \mathbb{N}$.

**Corollary A.2.** *$w_{2j+1} - (j+\frac{1}{4})\pi < e^{-2w_{2j+1}}$ and $w_{2j+2} - (j+\frac{3}{4})\pi > -e^{-2w_{2j+2}}$.*

*Proof.* For $w_{2j+1}$, use the relation $\tan(w_{2j+1}) = \coth(w_{2j+1}) = 1 + 2/(e^{2w_{2j+1}} - 1)$. We obtain that

$$w_{2j+1} - (j+\frac{1}{4})\pi < \tan(w_{2j+1} - (j+\frac{1}{4})\pi) = \frac{\tan(w_{2j+1}) - 1}{1 + \tan(w_{2j+1})} = e^{-2w_{2j+1}}.$$

The first inequality uses $x < \tan x$ for $x \in (0, \frac{\pi}{4})$. The other part of the corollary follows a similar derivation. □

### A.1 Proof of Theorem 2.1

*Proof.* The idea of proof comes from [39]. Define the operator $K^*$ by the kernel

$$\mathcal{G}^*(x,y) = \mathcal{G}(-1 + \frac{2}{n}\lfloor\frac{x+1}{2}\rfloor, -1 + \frac{2}{n}\lfloor\frac{y+1}{2}\rfloor)$$

where $\lfloor\cdot\rfloor$ is the floor function. We denote the eigenvalues of $K^*$ as $\mu_1^* \geq \mu_2^* \geq \cdots$, then for the equispaced biases $b_i^* = -1 + \frac{2(i-1)}{n}$, the corresponding Gram matrix $G^*$ has the eigenvalues exactly $\lambda_i^* = \frac{n}{2}\mu_i^*$. Using Weyl's inequality for self-adjoint compact operators

$$|\mu_i - \mu_i^*| \leq \|K - K^*\| = \sqrt{\int_{-1}^{1}\int_{-1}^{1} |\mathcal{G}(x,y) - \mathcal{G}^*(x,y)|^2 \, dxdy} = \mathcal{O}(n^{-1}). \tag{5}$$

Now we consider perturbed $\widetilde{b}_i = b_i^* + o(\frac{1}{n})$ as mentioned in Theorem 3.1, let the corresponding Gram matrix be $\widetilde{G}$, then by Weyl's inequality for Hermitian matrices

$$\|\lambda_i(\widetilde{G}) - \lambda_i(G^*)\| \leq \|\widetilde{G} - G^*\| \leq \sqrt{\sum_{i=1}^{n}\sum_{j=1}^{n} \left|\mathcal{G}(\widetilde{b}_i, \widetilde{b}_j) - \mathcal{G}(b_i^*, b_j^*)\right|^2} = o(1).$$

Therefore $|\lambda_i(\widetilde{G}) - \frac{n}{2}\mu_i| \leq C$ for some positive constant $C > 0$. □

**Lemma A.3.** *Suppose $\rho(x)$ is bounded from below and above and define*

$$\mathcal{G}_\rho(x,y) \coloneqq \rho(x)\mathcal{G}(x,y)\rho(y).$$

*Let $\widetilde{\mu}_k$ be the $k$-th eigenvalue of $\mathcal{G}_\rho$ in descending order, then $\inf_{[-1,1]}\rho \leq \widetilde{\mu}_k/\mu_k \leq \sup_{[-1,1]}\rho$.*

*Proof.* By Min-Max theorem for the eigenvalues of the integral kernel $\mathcal{G}_\rho$,

$$\widetilde{\mu}_k = \max_{S_k}\min_{z\in S_k, \|z\|=1}\int_{-1}^{1}\int_{-1}^{1}\mathcal{G}_\rho(x,y)z(x)z(y)dxdy,$$
$$\widetilde{\mu}_k = \min_{S_{k-1}}\max_{z\in S_{k-1}^\perp, \|z\|=1}\int_{-1}^{1}\int_{-1}^{1}\mathcal{G}_\rho(x,y)z(x)z(y)dxdy,$$

where $S_k$ is a $k$ dimensional subspace of $L^2[-1,1]$. In the first equation, we choose the space $S_k = \text{span}(\frac{\phi_1}{\rho}, \cdots, \frac{\phi_k}{\rho})$, where $(\mu_j, \phi_j)$ denotes the $j$th eigenpair of the kernel $\mathcal{G}$. Then let $z = \frac{1}{\rho}\sum_{j=1}^{k} c_j\phi_j, \|z\| = 1$, we find that

$$\widetilde{\mu}_k \geq \sum_{j=1}^{k}\mu_j c_j^2 \geq \mu_k\sum_{j=1}^{k}c_j^2 = \mu_k\|\rho z\| \geq \mu_k \inf\rho.$$

In the second equation, we choose the space $S_{k-1} = \text{span}(\rho\phi_1, \cdots, \rho\phi_{k-1})$ and let $z = \frac{1}{\rho}\sum_{j=k}^{\infty} c_j\phi_j \in S_{k-1}^\perp, \|z\| = 1$, then

$$\widetilde{\mu}_k \leq \sum_{j=k}^{\infty}\mu_j c_j^2 \leq \mu_k\sum_{j=k}^{\infty}c_j^2 = \mu_k\|\rho z\| \leq \mu_k \sup\rho.$$

□

### A.2 Proof of Corollary 2.2

*Proof.* This probabilistic argument is a straightforward application of Theorem 1 [37] estimating the eigenvalues of the kernel matrix, using the previous Lemma A.1 and Lemma A.3. □

## B Eigenvalues of Gram matrix in high dimension

Denote $V = \mathbb{S}^{d-1} \times [-1, 1]$, we consider the kernel $G : L^2(V) \mapsto L^2(V)$

$$G(\boldsymbol{w}, b, \boldsymbol{w}', b') = \int_D \sigma(\boldsymbol{w} \cdot \boldsymbol{x} - b)\sigma(\boldsymbol{w}' \cdot \boldsymbol{x} - b')d\boldsymbol{x}$$

Let $\phi_k(\boldsymbol{w}, b)$ be an eigenfunction for eigenvalue $\lambda_k$ which satisfies

$$\int_V G(\boldsymbol{w}, b, \boldsymbol{w}', b')\phi_k(\boldsymbol{w}', b')d\boldsymbol{w}'db' = \lambda_k\phi_k(\boldsymbol{w}, b). \tag{6}$$

One of the useful tools to study two-layer `ReLU` networks of infinite width is the Radon transform [23, 27]. Next, we construct the theory for the Gram matrix in the high dimension using the properties of the Radon transform.

**Definition B.1.** *Let $f : \mathbb{R}^d \to \mathbb{R}$ be an integrable function over all hyperplanes, the Radon transform*

$$\mathcal{R}f(\boldsymbol{w}, b) = \int_{\{\boldsymbol{x}|\boldsymbol{w}\cdot\boldsymbol{x}-b=0\}} f(\boldsymbol{x})dH_{d-1}(\boldsymbol{x}), \quad \forall\, (\boldsymbol{w}, b) \in \mathbb{S}^{d-1} \times \mathbb{R}.$$

*$H_{d-1}$ denotes the $(d-1)$ dimensional Lebesgue measure. The adjoint transform $\mathcal{R}^* : \mathbb{R}^d \to \mathbb{R}$ is*

$$\mathcal{R}^*\Phi(\boldsymbol{x}) \coloneqq \int_{\mathbb{S}^{d-1}} \Phi(\boldsymbol{w}, \boldsymbol{w} \cdot \boldsymbol{x})d\boldsymbol{w}, \quad \forall\, \boldsymbol{x} \in \mathbb{R}^d.$$

**Theorem B.2** (Helgason [12])**.** *The inversion formula of Radon transform is*

$$c_n f = (-\Delta)^{(d-1)/2}\mathcal{R}^*\mathcal{R}f,$$

*where $c_n = (4\pi)^{(d-1)/2}\frac{\Gamma(d/2)}{\Gamma(1/2)}$.*

Then we have the following lemma with Radon transform:

**Lemma B.3.** *The eigenfunction satisfies $\lambda_k\partial_b^2\phi_k = \mathcal{R}\Delta^{-1}\mathcal{R}^*\phi_k$ in weak sense.*

*Proof.* Differentiate (6) with $b$ twice and integrate against the test function

$$h \in \{\mathcal{R}g \mid \Delta^{-(d+1)/2}g \in C_0^2(D)\},$$

using $\partial_b^2\sigma(\boldsymbol{w} \cdot \boldsymbol{x} - b) = \delta(\boldsymbol{w} \cdot \boldsymbol{x} - b)$, we have

$$\int_D \int_V [\mathcal{R}^*h(\boldsymbol{x})]\, \sigma(\boldsymbol{w}' \cdot \boldsymbol{x} - b')\phi_k(\boldsymbol{w}', b')d\boldsymbol{w}'db'd\boldsymbol{x} = \lambda_k \int_V \partial_b^2\phi_k(\boldsymbol{w}, b)h(\boldsymbol{w}, b)d\boldsymbol{w}db. \tag{7}$$

Observe that the test function $h$ satisfies

$$(-\Delta)^{-1}\mathcal{R}^*h = (-\Delta)^{-(d+1)/2}(-\Delta)^{(d-1)/2}\mathcal{R}^*h = (-\Delta)^{-(d+1)/2}g \in C_0^2(D)$$

from the inversion formula of Radon transform in Theorem B.2. Using the Green's formula

$$\langle \mathcal{R}^*h(\boldsymbol{x}), \sigma(\boldsymbol{w}' \cdot \boldsymbol{x} - b')\rangle_D = \langle \Delta^{-1}\mathcal{R}^*h(\boldsymbol{x}), \Delta\sigma(\boldsymbol{w}' \cdot \boldsymbol{x} - b')\rangle_D = \mathcal{R}\Delta^{-1}\mathcal{R}^*h(\boldsymbol{w}', b'),$$

we derive that the right-hand side of (7) satisfies

$$\begin{aligned}\lambda_k \int_V \partial_b^2\phi_k(\boldsymbol{w}, b)h(\boldsymbol{w}, b)d\boldsymbol{w}db &= \int_V \mathcal{R}\Delta^{-1}\mathcal{R}^*h(\boldsymbol{w}', b')\phi_k(\boldsymbol{w}', b')d\boldsymbol{w}'db' \\ &= \int_V h(\boldsymbol{w}', b')\mathcal{R}\Delta^{-1}\mathcal{R}^*\phi_k(\boldsymbol{w}', b')d\boldsymbol{w}'db',\end{aligned}$$

where we have used the fact that $\mathcal{R}\Delta^{-1}\mathcal{R}^*$ is self-adjoint. □

**Lemma B.4** (Helgason [11], Lemma 2.1)**.** *These intertwining relations hold:* $\mathcal{R}\Delta = \partial_b^2\mathcal{R}$ *and* $\mathcal{R}^*\partial_b^2 = \Delta\mathcal{R}^*$.

Apply $\mathcal{R}^*$ on both sides of $\lambda_k\partial_b^2\phi_k = \mathcal{R}\Delta^{-1}\mathcal{R}^*\phi_k$, then

$$\lambda_k\mathcal{R}^*\phi_k = \Delta^{-1}\mathcal{R}^*\mathcal{R}\Delta^{-1}\mathcal{R}^*\phi_k$$

Therefore $(\lambda_k^{-1}, \mathcal{R}^*\phi_k)$ forms a pair of eigenvalue and eigenfunction of the operator $\Delta^{-1}\mathcal{R}^*\mathcal{R}\Delta^{-1}$. Therefore we only need to study the eigenvalues of $\Delta^{-1}\mathcal{R}^*\mathcal{R}\Delta^{-1}$. In the following proof, we show the eigenvalues decay as $\lambda_k = \Theta(k^{-(d+3)/d})$.

### B.1 Proof of Theorem 2.3

*Proof.* Using the inversion formula in Theorem B.2 and previous analysis, formally we obtain

$$\Delta^{-1}\mathcal{R}^*\mathcal{R}\Delta^{-1} = c_n(-\Delta)^{-(d+3)/2}$$

whose eigenvalues $\{\omega_k\}_{k\geq 1}$ are $\omega_k = \Theta(k^{-(d+3)/d})$ by exploiting the Weyl's law for $-\Delta$, if $(d+3)/2$ is fractional, one simply let the eigenfunction vanish outside $D$. □

**Remark B.5.** *For activation function* $\texttt{ReLU}^m(x) = \frac{1}{m!}[\max(x,0)]^m$ *in d-dimension with* $m \geq 1$*, one can modify the above argument to formally show:*

- *If* $m$ *is odd,* $(\lambda_k^{-1}, \mathcal{R}^*\phi_k)$ *forms an eigenpair of the operator* $\Delta^{-\frac{m+1}{2}}\mathcal{R}^*\mathcal{R}\Delta^{-\frac{m+1}{2}}$.
- *If* $m$ *is even,* $(\lambda_k^{-1}, \mathcal{R}^*\partial_b\phi_k)$ *forms an eigenpair of* $-\Delta^{-\frac{m}{2}}\mathcal{R}^*\mathcal{R}\Delta^{-\frac{m+2}{2}}$.

*Using the inversion formula for the Radon transform, we have* $\lambda_k = \Theta(k^{-\frac{d+2m+1}{d}})$.

## C Learning Dynamics for 1D

### C.1 Mathematical setup of the learning dynamics

Let $D = (-1, 1)$, we consider approximating the objective function $f(x) \in C(D)$, with the shallow neural network

$$h(x) = \sum_{i=1}^n a_i\sigma(x - b_i).$$

Generally speaking, the biases $\{b_i\}_{i=1}^n$ are supported on $\mathbb{R}$ during the training process. For analysis purposes, it is much easier to consider the simple scenario that $\{b_i\}_{i=1}^n \subseteq D$. We relax the setting to the following form of neural network

$$h(x) = \sum_{i=1}^n a_i\psi(x, b_i), \quad \psi(x, b_i) = \chi(b_i)\sigma(x-b_i), \quad \partial_x^2\psi(x,b) = \partial_b^2\psi(x,b) = \delta(x-b),\ x, b \in D,$$

where $\chi$ is an approximation to the characteristic function of $D$ by adding a quadratic transition region:

$$\chi(x) = \begin{cases} 1 & x \in D, \\ 1 - \left(\frac{1}{\varepsilon}(x+1)\right)^2 & x \in (-1-\varepsilon, -1], \\ 0 & \text{otherwise}, \end{cases}$$

where $\varepsilon$ is a positive parameter. We denote $D^\varepsilon = \operatorname{supp}\chi = (-1-\varepsilon, 1)$. The loss function is

$$\mathcal{L}(h, f) \coloneqq \frac{1}{2}\int_D |h(x) - f(x)|^2 dx.$$

Minimizing $\mathcal{L}(h, f)$ over the parameters $\{a_i\}_{i\in[n]}$ and $\{b_i\}_{i\in[n]}$ with gradient descent can be represented by the gradient flow which follows the equations

$$\frac{d}{dt}a_i(t) = -\int_D (h(x,t) - f(x))\psi(x, b_i(t))dx \tag{8}$$

and

$$\frac{d}{dt}b_i(t) = -a_i(t)\int_D (h(x,t) - f(x))\partial_b\psi(x, b_i(t))dx \tag{9}$$

with certain initial conditions $\{a_i(0)\}_{i\in[n]}$ and $\{b_i(0)\}_{i\in[n]}$.

**Theorem C.1.** *If the initial biases $\{b_i(0)\}_{i\in[n]} \subseteq D^\varepsilon$ and weights $\sup_{i\in[n]}|a_i(0)| < \infty$. Then $\{b_i(t)\}_{i\in[n]} \subseteq \overline{D^\varepsilon}$, $\forall\, t \geq 0$.*

*Proof.* At any time $t$, using Cauchy-Schwartz inequality,

$$\begin{aligned}\left|\frac{d}{dt}a_i(t)\right| &\leq \sqrt{\int_D |h(x,t) - f(x)|^2 dx}\sqrt{\int_D \psi(x, b_i(t))^2 dx} \\ &\leq \sqrt{\int_D |h(x,0) - f(x)|^2 dx}\sqrt{\int_D \psi(x, b_i(t))^2 dx} \quad < \infty.\end{aligned}$$

Therefore if the initialization of every $a_i(0)$ is finite, $a_i(t)$ is always finite, which in turn implies every derivative $\frac{d}{dt}b_i(t)$ is also finite. Suppose at time $t > 0$ that $b_k(t) \in \overline{D^\varepsilon}^{\complement}$, then there exists an open path that $\forall\, t' \in (t_0, t_1) \subseteq (0, t)$ that $\frac{d}{dt}b_k(t') \neq 0$ and $b_k(t') \in \overline{D^\varepsilon}^{\complement}$. However, $\partial_b\psi(x, b) = 0$ for $b \in \overline{D^\varepsilon}^{\complement}$, which is a contradiction. Therefore every $\{b_i(t)\}_{i\in[n]} \subseteq \overline{D^\varepsilon}$.

□

Although the gradient flow (8) and (9) makes the dynamics of biases $\{b_i\}_{i\in[n]}$ supported on $D^\varepsilon$, one potential issue is the accumulation of biases towards the transition region $D^\varepsilon - D$, which might deteriorate the approximate accuracy.

**Remark C.2.** *When the initialization $\{(a_i(0), b_i(0))\}_{i\in[n]}$ is densely distributed on $K \subseteq \mathbb{R}\times D^\varepsilon$, one can assign an empirical measure for the biases $\mu(a, b, t) = \frac{1}{n}\sum_{i=1}^n \delta(a - a_i(t), b - b_i(t))$, the dynamics can be viewed as a continuous mapping $X_t : \mathcal{P}(\mathbb{R}\times D^\varepsilon) \to \mathcal{P}(\mathbb{R}\times D^\varepsilon)$ that*

$$X_t(\mu(a, b, 0)) = \mu(a, b, t).$$

*where $\mathcal{P}$ represents the admissible measure space. In the limit $n \to \infty$, $\operatorname{supp}\mu(\cdot,\cdot, 0)$ will be homeomorphic to $\operatorname{supp}\mu(\cdot,\cdot, t)$. Since the boundary $\mathbb{R}\times\partial D^\varepsilon$ is fixed under $X_t$, therefore if $K$ separates the sets $\{-A\}\times\mathring{D}^\varepsilon$ and $\{A\}\times\mathring{D}^\varepsilon$ for certain $A > 0$, then the marginal distribution $\int_{\mathbb{R}}\mu(da, b, t)$ must have a full support on $D^\varepsilon$.*

Let $\phi_k$ be an eigenfunction with eigenvalue $\lambda_k \geq 0$ (arranged in descending order) of the Gram kernel $\mathcal{G}(b, b')$ on $D^\varepsilon \times D^\varepsilon$ defined by

$$\mathcal{G}(b, b') = \int_D \psi(x, b)\psi(x, b')dx,$$

which is a compact operator in $L^2(D^\varepsilon)$. Then $\mathcal{G}(b, b') = \sum_{k\geq 1}\lambda_k\phi_k(b)\phi_k(b')$ and the properties of $(\lambda_k, \psi_k)$ will be elaborated later. Using the eigenfunction as a test function, we can derive

$$\begin{aligned}\frac{d}{dt}\sum_{i=1}^n a_i(t)\phi_k(b_i(t)) &= \sum_{i=1}^n \phi(b_i(t))\frac{da_i}{dt} + \sum_{i=1}^n a_i(t)\phi_k'(b_i(t))\frac{db_i}{dt} \\ &= -\sum_{i=1}^n \phi_k(b_i(t))\int_D (h(x,t) - f(x))\,\psi_k(x, b_i(t))dx \\ &\quad -\sum_{i=1}^n \phi'(b_i(t))|a_i(t)|^2\int_D (h(x,t) - f(x))\partial_b\psi_k(x, b_i(t))dx \\ &= -\sum_{i=1}^n \phi_k(b_i(t))\left(\sum_{j=1}^n G_{ij}(t)a_j(t) - P(b_i(t))\right) \\ &\quad -\sum_{i=1}^n |a_i(t)|^2\phi_k'(b_i(t))\left(\sum_{j=1}^n K_{ij}(t)a_j(t) - Q(b_i(t))\right).\end{aligned}$$

where $G = (G_{ij})_{i,j\in[n]}$ and $K = (K_{ij})_{i,j\in[n]}$ are

$$G_{ij}(t) = \mathcal{G}(b_i(t), b_j(t)), \quad K_{ij}(t) = \partial_b \mathcal{G}(b_i(t), b_j(t)).$$

The functions $P$ and $Q$ are

$$P(b) = \int_D f(x)\psi(x,b)dx, \quad Q(b) = \int_D f(x)\partial_b\psi(x,b)dx.$$

We can represent $P(b)$ and $Q(b)$ as sum of eigenfunctions on $D^\varepsilon$ as well:

$$P(b) = \sum_{k\geq 1} p_k \phi_k(b), \quad Q(b) = \sum_{k\geq 1} p_k \phi_k'(b).$$

Therefore we can derive that

$$\begin{aligned}
&-\sum_{i=1}^n \phi_k(b_i(t)) \left( \sum_{j=1}^n G_{ij}(t)a_j(t) - P(b_i(t)) \right) \\
&= -\sum_{l=1}^\infty \sum_{i=1}^n \phi_k(b_i(t))\phi_l(b_i(t)) \left[ \lambda_l \sum_{j=1}^n \phi_l(b_j(t))a_j(t) - p_l \right]
\end{aligned}$$

and

$$\begin{aligned}
&-\sum_{i=1}^n |a_i(t)|^2 \phi_k'(b_i(t)) \left( \sum_{j=1}^n K_{ij}(t)a_j(t) - Q(b_i(t)) \right) \\
&= -\sum_{l=1}^\infty \sum_{i=1}^n |a_i(t)|^2 \phi_k'(b_i(t))\phi_l'(b_i(t)) \left[ \lambda_l \sum_{j=1}^n \phi_l(b_j(t))a_j(t) - p_l \right].
\end{aligned}$$

Denote $\Theta_k(t) = \sum_{j=1}^n \phi_k(b_j(t))a_j(t) - \frac{p_k}{\lambda_k}$, we find that

$$\frac{d\Theta_k(t)}{dt} = -\sum_{l=1}^\infty \lambda_l \left[ M_{lk}(t) + S_{lk}(t) \right] \Theta_l(t) \tag{10}$$

where the infinite matrices

$$M_{lk}(t) = \sum_{i=1}^n \phi_l(b_i(t))\phi_k(b_i(t)), \quad S_{lk}(t) = \sum_{i=1}^n |a_i(t)|^2 \phi_k'(b_i(t))\phi_l'(b_i(t))$$

are both semi-positive.

### C.1.1 Convergence

To study the convergence, consider the energy $E(t) = \frac{1}{2}\sum_{k\geq 1} \lambda_k |\Theta_k^2(t)|$, then

$$\frac{dE(t)}{dt} = -\sum_{k,l=1}^\infty \lambda_k\lambda_l \Theta_k(t) \left[ M_{lk}(t) + S_{lk}(t) \right] \Theta_l(t).$$

Since the matrices are both non-negative, the energy is non-increasing, thus there is a limit for $E(t)$ as $t \to \infty$. Define the auxiliary function

$$w(b,t) \coloneqq \sum_{k=1}^\infty \lambda_k \Theta_k(t)\phi_k(b), \tag{11}$$

which is directly related to the error from the following relation for $b \in D$,

$$\begin{aligned}
\partial_b^2 w(b,t) &= \partial_b^2 \left[ \sum_{k=1}^{\infty} \left( \lambda_k \sum_{j=1}^{n} \phi_k(b_j(t)) a_j(t) - p_k \right) \phi_k(b) \right] \\
&= \partial_b^2 \left[ \sum_{j=1}^{n} \mathcal{G}(b, b_j(t)) a_j(t) - P(b) \right] \\
&= \partial_b^2 \left[ \sum_{j=1}^{n} a_j(t) \int_D \psi(x,b)\psi(x,b_j(t))dx - \int_D f(x)\psi(b)dx \right] \\
&= \sum_{j=1}^{n} a_j(t) \int_D \delta(x-b)\psi(x,b_j(t))dx - \int_D f(x)\delta(x-b)dx = h(b,t) - f(b).
\end{aligned} \tag{12}$$

We first provide its regularity property which can be related to the spectral decay of the Gram matrix determined by the regularity of the activation function.

**Lemma C.3.** *$\phi_k$ is a cubic polynomial over $(-1-\varepsilon, -1)$ and*

$$\partial_b^4 \phi_k(b) = \begin{cases} 0, & b \in (-1-\varepsilon, -1) \\ \lambda_k^{-1} \phi_k(b), & b \in (-1, 1) \end{cases} \tag{13}$$

*where $\partial_b \phi_k$ is continuous at $b = -1$ but $\partial_b^2 \phi_k$ has a jump at $b = -1$.*

*Proof.* We use the definition of eigenfunction

$$\int_{D^\varepsilon} \mathcal{G}(b,b')\phi_k(b')db' = \lambda_k \phi_k(b).$$

For $b \in (-1,1)$, $\chi(b) = 1$, then differentiating both sides

$$\lambda_k \partial_b^4 \phi_k(b) = \partial_b^4 \int_{D^\varepsilon} \int_D \sigma(x-b)\sigma(x-b')\chi(b')\phi_k(b')dxdb' = \int_{D^\varepsilon} \delta(b-b')\chi(b')\phi_k(b')db' = \phi_k(b).$$

For $b \in (-1-\varepsilon, -1)$, $\chi(b)$ is quadratic, $\sigma(x-b) = x - b$ for $x \in D$, we differentiate both sides

$$\lambda_k \partial_b^4 \phi_k(b) = \partial_b^4 \left( \chi(b) \int_{D^\varepsilon} \int_D (x-b)\sigma(x-b')\chi(b')\phi_k(b')dxdb' \right) = 0.$$

Now, we compute $\partial_b \phi_k$ and $\partial_b^2 \phi_k$ across $b = -1$. Note $\chi'(-1) = 0$, then

$$\begin{aligned}
\lim_{b \to -1^-} \partial_b \phi_k(b) &= \frac{1}{\lambda_k} \lim_{b \to -1^-} \partial_b \left( \chi(b) \int_{D^\varepsilon} \int_D (x-b)\sigma(x-b')\chi(b')\phi_k(b')dxdb' \right) \\
&= \frac{1}{\lambda_k} \chi'(-1) \lim_{b \to -1^-} \left( \int_{D^\varepsilon} \int_D (x-b)\sigma(x-b')\chi(b')\phi_k(b')dxdb' \right) \\
&\quad + \frac{1}{\lambda_k} \chi(-1) \lim_{b \to -1^-} \left( \int_{D^\varepsilon} \int_D (-1)\sigma(x-b')\chi(b')\phi_k(b')dxdb' \right) \\
&= \frac{1}{\lambda_k} \left( \int_{D^\varepsilon} \int_D (-1)\sigma(x-b')\chi(b')\phi_k(b')dxdb' \right)
\end{aligned}$$

and because $\sigma'(x-b) = 1$ if $b = -1$ and $x \in D$.

$$\begin{aligned}
\lim_{b \to -1^+} \partial_b \phi_k(b) &= \frac{1}{\lambda_k} \lim_{b \to -1^+} \partial_b \left( \int_{D^\varepsilon} \int_D \sigma(x-b)\sigma(x-b')\chi(b')\phi_k(b')dxdb' \right) \\
&= \frac{1}{\lambda_k} \lim_{b \to -1^+} \left( \int_{D^\varepsilon} \int_D -\sigma'(x-b)\sigma(x-b')\chi(b')\phi_k(b')dxdb' \right) \\
&= \frac{1}{\lambda_k} \left( \int_{D^\varepsilon} \int_D (-1)\sigma(x-b')\chi(b')\phi_k(b')dxdb' \right).
\end{aligned}$$

For $\partial_b^2\phi_k$ across $b=-1$, following a similar process,

$$\begin{aligned}\lim_{b\to -1^-}\partial_b^2\phi_k(b) &= \frac{1}{\lambda_k}\lim_{b\to -1^-}\partial_b^2\left(\chi(b)\int_{D^\varepsilon}\int_D (x-b)\sigma(x-b')\chi(b')\phi_k(b')dxdb'\right)\\ &= \frac{1}{\lambda_k}\chi''(-1)\lim_{b\to -1^-}\left(\int_{D^\varepsilon}\int_D (x-b)\sigma(x-b')\chi(b')\phi_k(b')dxdb'\right)\\ &= -\frac{1}{\lambda_k}\frac{2}{\varepsilon^2}\left(\int_{D^\varepsilon}\int_D (x+1)\sigma(x-b')\chi(b')\phi_k(b')dxdb'\right)\end{aligned}$$

and

$$\begin{aligned}\lim_{b\to -1^+}\partial_b^2\phi_k(b) &= \frac{1}{\lambda_k}\lim_{b\to -1^+}\partial_b^2\left(\int_{D^\varepsilon}\int_D \sigma(x-b)\sigma(x-b')\chi(b')\phi_k(b')dxdb'\right)\\ &= \frac{1}{\lambda_k}\lim_{b\to -1^+}\left(\int_{D^\varepsilon}\int_D \delta(x-b)\sigma(x-b')\chi(b')\phi_k(b')dxdb'\right)\\ &= \frac{1}{\lambda_k}\int_{D^\varepsilon}\sigma(-1-b')\chi(b')\phi_k(b')db'\\ &= \frac{1}{\lambda_k}\int_{-1-\varepsilon}^{-1}(-1-b')\chi(b')\phi_k(b')db'.\end{aligned}$$

As $\varepsilon\to 0$, $\lim_{b\to -1^+}\partial_b^2\phi_k(b)=O(\varepsilon)$ while $\lim_{b\to -1^-}\partial_b^2\phi_k(b)=O(\varepsilon^{-2})$. □

**Theorem C.4.** *The auxiliary function $w\in H^1(D^\varepsilon)$ and $w\in H^2(D)$ uniformly, respectively.*

*Proof.* From (12), we have $\|\partial_b^2 w\|_{L^2(D)}\le \|h(\cdot,0)-f(\cdot)\|_{L^2(D)}$ uniformly. We also notice that each eigenfunction $\phi_k$, $k\in\mathbb{N}$ satisfies that $\phi_k(b,t)|_{b=1}=\partial_b\phi_k(b,t)|_{b=1}=0$, hence $w(b,t)|_{b=1}=\partial_b w(1,t)=0$. Using Cauchy-Schwartz inequality, we derive the following Poincaré inequalities,

$$\|w(b,t)\|_{L^2(D)}^2=\left\|\int_1^b \partial_b w(b',t)db'\right\|_{L^2(D)}^2\le 2\left\|\partial_b w(b,t)\right\|_{L^2(D)}^2.$$

and

$$\|\partial_b w(b,t)\|_{L^2(D)}^2=\left\|\int_1^b \partial_b^2 w(b',t)db'\right\|_{L^2(D)}^2\le 2\left\|\partial_b^2 w(b,t)\right\|_{L^2(D)}^2.$$

Therefore $w\in H^2(D)$. Now we prove the other part of the theorem: $w\in H^1(D^\varepsilon)$ uniformly. Here we use the fact that $E(t)=\frac{1}{2}\sum_{k\in\mathbb{N}}\lambda_k|\Theta_k(t)|^2$ is uniformly bounded by $E(0)$, then

$$\|w(\cdot,t)\|_{L^2(D)}^2\le\sum_{k\in\mathbb{N}}\lambda_k^2|\Theta_k(t)|^2<\lambda_1\sum_{k\in\mathbb{N}}\lambda_k|\Theta_k(t)|^2\le\lambda_1 E(0).$$

Follow the same derivation of (12),

$$\begin{aligned}\partial_b w(b,t) &= \partial_b\left[\sum_{k=1}^\infty\left(\lambda_k\sum_{j=1}^n\phi_k(b_j(t))a_j(t)-p_k\right)\phi_k(b)\right]\\ &= \partial_b\left(\sum_{j=1}^n\mathcal{G}(b,b_j(t))a_j(t)-P(b)\right)\\ &= \partial_b\left(\sum_{j=1}^n a_j(t)\int_D\psi(x,b)\psi(x,b_j(t))dx-\int_D f(x)\psi(x,b)dx\right)\\ &= \sum_{j=1}^n a_j(t)\int_D\partial_b\psi(x,b)\psi(x,b_j(t))dx-\int_D f(x)\partial_b\psi(x,b)dx\\ &= \int_D\left(h(x,t)-f(x)\right)\partial_b\psi(x,b)dx.\end{aligned}$$

Thus using $\|h(\cdot,t)-f\|_{L^2(D)} \le \|h(\cdot,0)-f\|_{L^2(D)}$ and $\partial_b\psi(x,b)\in C^0(D\times D^\varepsilon)$, the following inequality holds uniformly:

$$\|\partial_b w(b,t)\|^2_{L^2(D^\varepsilon)} \le \|h(\cdot,0)-f\|^2_{L^2(D)} \int_{D\times D^\varepsilon} |\partial_b\psi(x,b)|^2 dxdb < \infty.$$

□

Let $\{E(t_m)\}_{m\ge 1}$ be a minimizing sequence for $E(t)$, then

$$\begin{aligned}&\sum_{k,l=1}^{\infty} \lambda_k\lambda_l\Theta_k(t_m)[M_{lk}(t_m)+S_{lk}(t_m)]\Theta_l(t_m)\\ =&\sum_{i=1}^{n}\left(|w(b_i(t_m),t_m)|^2 + a_i^2(t_m)|\partial_b w(b_i(t_m),t_m)|^2\right)\to 0,\end{aligned}$$

which implies that $w(b_i(t_m),t_m)\to 0$ and $|a_i(t_m)\partial_b w(b_i(t_m),t_m)|\to 0$. Note that $H^1(D^\varepsilon)$ embeds into $L^2(D^\varepsilon)$ compactly, there exists a subsequence $\{w(\cdot,t_{m_s})\}_{s\ge 1}$ converges to $\bar w\in H^1(D^\varepsilon)$ strongly (which is in $C^{0,\alpha}(D^\varepsilon)$). Here are two cases:

1. If the gradient dynamics $b_i(t)$ converges to $b_i^*$ as $t\to\infty$, then we must have $\bar w(b_i^*)=0$. If $\lim_{t\to\infty} a_i(t)\neq 0$ or does not exists, then $\partial_b\bar w(b_i^*)=0$.
2. If during the dynamics $b_i(t)$ is not converging, then there exists an open set $T\subseteq D^\varepsilon$ that $T\subseteq \limsup_{\tau\to\infty}\{b_i(t)\}_{t\ge\tau}$ or equivalently, $T$ appears infinitely often in the dynamics. Then we must have $\bar w(b)=0, \forall\, b\in T$.

**Remark C.5.** *In mean-field representation that $n\to\infty$ and assume the limiting measure $\int_{\mathbb{R}}\mu(da,b,t)$ has full support on $D^\varepsilon$, we immediately conclude that $\bar w\equiv 0$. Hence $\Theta_k(t)\to 0$ and $E(t)\to 0$ as $t\to\infty$. This implies the network will converge to the objective function. However, in a discrete setting, it becomes more complicated due to the existence of local minimums.*

### C.2 Generalized Fourier analysis of the convergence

In this section, we study the convergence of the learning dynamics in terms of frequency modes, especially the asymptotic behavior for high-frequency components. The key relation is (12), which implies one can study the evolution of the Fourier modes of $\partial_b^2 w(b,t)$ to understand the evolution of error $h(b,t)-f(b)$. The other key relation is (13), which will provide a Fourier mode decay rate in the error. However, due to the bounded domain of interest $b\in D$ and non-periodicity at the boundary, generalized Fourier modes have to be designed for our study.

#### C.2.1 Generalized Fourier modes

In order to handle the boundary values, we introduce an orthonormal basis (prove later) $\theta_k(x)\in C(D)$ that solves the eigenvalue problem

$$\begin{aligned}\theta_k^{(4)}(x) &= p_k\theta_k(x),\\ \theta_k(1)=\theta_k'(1)&=0,\\ \theta_k''(-1)=\theta_k'''(-1)&=0.\end{aligned}\tag{14}$$

**Lemma C.6.** *The eigenfunction $\theta_k$ satisfies*

$$\theta_k(x) = A_k\cosh(c_kx)+B_k\sinh(c_kx)+C_k\cos(c_kx)+D_k\sin(c_kx).$$

*where* $\tanh(c_k)\tan(c_k)=\pm 1$, $p_k=c_k^4$, *and* $c_{2k+1}\in((k+\frac14)\pi,(k+\frac12)\pi)$, $c_{2k+2}\in((k+\frac12)\pi,(k+\frac34)\pi)$, $k\ge 0$.

*Proof.* The form of the eigenfunction is standard. Using the boundary conditions, $\theta_k(1)=\theta_k''(-1)=0$,

$$\begin{aligned}A_k\cosh(c_k)+B_k\sinh(c_k)+C_k\cos(c_k)+D_k\sin(c_k)&=0\\ A_k\cosh(c_k)-B_k\sinh(c_k)-C_k\cos(c_k)+D_k\sin(c_k)&=0\end{aligned}$$

which means

$$A_k \cosh(c_k) + D_k \sin(c_k) = 0, \quad B_k \sinh(c_k) + C_k \cos(c_k) = 0.$$

The other two boundary condutions are

$$\begin{aligned} A_k \sinh(c_k) + B_k \cosh(c_k) - C_k \sin(c_k) + D_k \cos(c_k) = 0 \\ -A_k \sinh(c_k) + B_k \cosh(c_k) - C_k \sin(c_k) - D_k \cos(c_k) = 0 \end{aligned}$$

which means

$$A_k \sinh(c_k) + D_k \cos(c_k) = 0, \quad B_k \cosh(c_k) - C_k \sin(c_k) = 0.$$

If $C_k \neq 0$, then $B_k = -C_k \frac{\cos(c_k)}{\sinh(c_k)} = C_k \frac{\sin(c_k)}{\cosh(c_k)}$, which is $\tan(c_k)\tanh(c_k) = -1$. If $D_k \neq 0$, then we can derive $\tan(c_k)\tanh(c_k) = 1$. Let $r(x) = \tan(x)\tanh(x)$, for $x \in (0, \frac{\pi}{2})$ or $x \in (n\pi + \frac{1}{2}\pi, n\pi + \frac{3\pi}{2})$, $n \in \mathbb{Z}$, the function $r$ is monotone, therefore $c_{2k+1} \in ((k+\frac{1}{4})\pi, (k+\frac{1}{2})\pi)$, $c_{2k+2} \in ((k+\frac{1}{2})\pi, (k+\frac{3}{4})\pi)$, $k \geq 0$. □

From the above analysis, the eigenfunctions are

$$\begin{aligned} \theta_{2k+1}(x) &= C_{2k+1}\left(-\frac{\cos(c_{2k+1})}{\sinh(c_{2k+1})}\sinh(c_{2k+1}x) + \cos(c_{2k+1}x)\right), \\ \theta_{2k+2}(x) &= D_{2k+2}\left(-\frac{\sin(c_{2k+2})}{\cosh(c_{2k+2})}\cosh(c_{2k+2}x) + \sin(c_{2k+2}x)\right), \end{aligned}$$

which shows $\{\theta_k\}_{k\geq 1}$ are actually the eigenfunctions of the Gram kernel $\mathcal{G}$ in (3).

**Lemma C.7.** *$\{\theta_k\}_{k\geq 1}$ forms an orthonormal basis of $L^2(D)$.*

*Proof.* Since each eigenvalue is simple from Corollary A.2 and we verify the following equality using integration by parts,

$$p_i \int_D \theta_i(x)\theta_j(x)dx = \int_D \theta_i^{(4)}(x)\theta_j(x)dx = \int_D \theta_i(x)\theta_j^{(4)}(x)dx = p_j \int_D \theta_i(x)\theta_j(x)dx.$$

Thus $\{\theta_i\}_{i\geq 1}$ forms an orthonormal basis. □

**Lemma C.8.** *The eigenfunctions $\{\theta_k\}_{k\geq 1}$ can form a complete basis for $L^2(D)$.*

*Proof.* Suppose $\{\theta_m\}_{m=1}^{\infty}$ is not complete, then there exists a nonzero $\gamma \in L^2(D)$ that $\widehat{\gamma}(m) = 0$ for all $m \in \mathbb{N}$, then using the fact that $\{\theta_m\}_{m\geq 1}$ are the eigenfunctions of the Gram kernel $\mathcal{G}$ in (3), note $\mathcal{G}(x,y) = \mathcal{G}(y,x)$, it is self-adjoint, then by Hilbert-Schmidt theorem,

$$\int_D \mathcal{G}(x,y)\gamma(y)dy = 0 \tag{15}$$

and we differentiate the above equation 4 times on both sides, which leads to $\gamma^{(4)}(x) = 0$ which means $\gamma$ should be a cubic polynomial with boundary conditions $\gamma(1) = \gamma'(1) = \gamma''(-1) = \gamma'''(-1) = 0$, which means $\gamma \equiv 0$, it is a contradiction with our assumption of $\|\gamma\|_D \neq 0$. □

Next, we show the eigenfunctions are *almost* Fourier modes with a shifted frequency.

**Theorem C.9.** *The following statements hold*

1. *$A_k, B_k = \mathcal{O}(e^{-c_k})$ and $C_k, D_k = \mathcal{O}(1)$.*
2. *$\|\theta_k\|_{L^\infty(D)} = \mathcal{O}(1)$, $\|\theta_k'\|_{L^\infty(D)} = \mathcal{O}(k)$ and $\|\theta_k''\|_{L^\infty(D)} = \mathcal{O}(k^2)$.*
3. *$\|\theta_{2k+1}(x) - \cos(c_{2k+1}x)\|_{L^2(D)} = \mathcal{O}(k^{-1/2})$ and $\|\theta_{2k+2}(x) - \sin(c_{2k+2}x)\|_{L^2(D)} = \mathcal{O}(k^{-1/2})$*

*Proof.* We only prove for $\theta_{2k+1}$, the proof is similar for $\theta_{2k+2}$. Using the symmetry of the domain $D$,

$$\begin{aligned}
&\int_D \left(-\frac{\cos(c_{2k+1})}{\sinh(c_{2k+1})}\sinh(c_{2k+1}x)+\cos(c_{2k+1}x)\right)^2 dx \\
&= \int_D \left(\frac{\cos(c_{2k+1})}{\sinh(c_{2k+1})}\sinh(c_{2k+1}x)\right)^2 dx + \int_D \cos^2(c_{2k+1}x)dx \\
&\quad - 2\int_D \frac{\cos(c_{2k+1})}{\sinh(c_{2k+1})}\sinh(c_{2k+1}x)\cos(c_{2k+1}x)dx \\
&= \left(\frac{\cos(c_{2k+1})}{\sinh(c_{2k+1})}\right)^2\left[\frac{\sinh(2c_{2k+1})}{2c_{2k+1}}-1\right]+\left[\frac{\sin(2c_{2k+1})}{2c_{2k+1}}+1\right] \\
&= \frac{\cos^2(c_{2k+1})\coth(c_{2k+1})}{c_{2k+1}}+\frac{\sin(2c_{2k+1})}{2c_{2k+1}}+1-\left(\frac{\cos(c_{2k+1})}{\sinh(c_{2k+1})}\right)^2 \\
&= 1+\mathcal{O}(k^{-1}).
\end{aligned} \tag{16}$$

Therefore $C_{2k+1} = 1+\mathcal{O}(k^{-1})$ and $|B_{2k+1}| \le \sinh(c_{2k+1})^{-1}|C_{2k+1}| = \mathcal{O}(e^{-c_{2k+1}})$. The norm $\|\theta_{2k+1}\|_{L^\infty(D)} \le 2C_{2k+1} = \mathcal{O}(1)$ and

$$\theta'_{2k+1}(x) = C_{2k+1}c_{2k+1}\left(-\frac{\cos(c_{2k+1})}{\sinh(c_{2k+1})}\cosh(c_{2k+1}x)-\sin(c_{2k+1}x)\right),$$

which means $\|\theta'_{2k+1}\|_{L^\infty(D)} = \mathcal{O}(k)$ and similarly, $\|\theta''_{2k+1}\|_{L^\infty(D)} = \mathcal{O}(k^2)$. We also can see from (16) that

$$\int_D |\theta_{2k+1}(x) - C_{2k+1}\cos(c_{2k+1}x)|^2 dx = \mathcal{O}(k^{-1}).$$

which means $\theta_k \sim C_{2k+1}\cos(c_{2k+1}x)+\mathcal{O}(k^{-1/2}) = \cos(c_{2k+1}x)+\mathcal{O}(k^{-1/2})$. □

### C.2.2 Generalized discrete Fourier analysis

Let $\widehat{w}$ denote the *generalized* discrete Fourier transform of $w$ on $D$:

$$\widehat{w}(k,t) = \int_D \theta_k(b)w(b,t)db. \tag{17}$$

where $\theta_k$ is the eigenfunction from (14), which is close to the shifted Fourier modes when $k$ is relatively large. We emphasize the following key property related to the activation function $\partial_b^2 w(b,t) = h(b,t) - f(b)$ for $b \in D$ by (12). Therefore the generalized discrete Fourier transform of $\partial_b^2 w$ will be the generalized discrete Fourier transform of the error $h(\cdot,t) - f(\cdot)$ on $D$. Using Lemma C.3, $\partial_b^4 w(b,t) = \sum_{k=1}^\infty \Theta_k(t)\phi_k(b)$ for $b \in D$.

**Lemma C.10.** *The following equality holds.*

$$\int_D w(b,t)\theta_k^{(4)}(b)db = \int_D \partial_b^2 w(b,t)\theta_k''(b)db.$$

*Proof.* Note $\theta_k''(-1) = \theta_k'''(-1) = 0, w(1,t) = \partial_b w(1,t) = 0$ (due to $\phi_k(1) = \phi_k'(1) = 0$),

$$\begin{aligned}
\int_D w(b,t)\theta_k^{(4)}(b)db &= w(b,t)\theta_k^{(3)}(b)\big|_{\partial D} - \int_D \partial_b w(b,t)\theta_k^{(3)}(b)db \\
&= -\partial_b w(b,t)\theta_k^{(2)}(b)\big|_{\partial D} + \int_D \partial_b^2 w(b,t)\theta_k''(b)db \\
&= \int_D \partial_b^2 w(b,t)\theta_k''(b)db.
\end{aligned}$$

□

**Lemma C.11.** *There exists a constant $c > 0$ that $|\widehat{w}(k,t)| \le ck^{-2}$.*

*Proof.* Using $\theta_k^{(4)}(b) = p_k\theta_k(b)$, we have

$$|p_k\widehat{w}(k,t)| \le \int_D |\partial_b^2 w(b,t)\theta_k''(b)|db \le \|h(\cdot,0) - f(\cdot)\|_{L^2(D)}\|\theta_k''\|_{L^2(D)}.$$

Since $\|\theta_k''\|_{L^2(D)} = \mathcal{O}(k^2)$, there exists a constant $c > 0$ that $|\widehat{w}(k,t)| \le \frac{c}{k^2}$. □

From now on, we assume that $b_i(t)$ is arranged in ascending order. Let $s = s(t)$ be the smallest index such that $\{b_j(t)\}_{j\ge s} \subseteq D$. Then use integration by parts taking into account the boundary condition of $\theta_k, w$ and the fact $\partial_b^2 w(b,t) = h(b,t) - f(b)$,

$$\begin{aligned}
\int_D \theta_k(b)\partial_b^4 w(b,t)db &= \theta_k(b)\partial_b^3 w(b,t)\Big|_{\partial D} - \int_D \theta_k'(b)\partial_b^3 w(b,t)db \\
&= \theta_k(b)\partial_b^3 w(b,t)\Big|_{\partial D} - \theta_k'(b)\partial_b^2 w|_{\partial D} + \int_D \theta_k''(b)\partial_b^2 w(b,t)db \\
&= \theta_k(b)\partial_b^3 w(b,t)\Big|_{\partial D} - \theta_k'(b)\partial_b^2 w|_{\partial D} - \int_D \theta_k'''(b)\partial_b w(b,t)db \\
&= \theta_k(b)\partial_b^3 w(b,t)\Big|_{\partial D} - \theta_k'(b)\partial_b^2 w|_{\partial D} + \int_D \theta_k^{(4)} w(b,t)db \\
&= \theta_k(b)\partial_b^3 w(b,t)\Big|_{\partial D} - \theta_k'(b)\partial_b^2 w|_{\partial D} + p_k\widehat{w}(k,t).
\end{aligned}$$

In order to handle the first term later, we need the following summation

$$\mathcal{H}_k(t) \coloneqq \theta_k(b)\partial_b^3 h(b,t)\Big|_{\partial D} = -\theta_k(-1)\sum_{l=1}^{s-1} a_l(t)(-\chi(b_l(t)) + \chi'(b_l(t))(-1 - b_l(t))). \tag{18}$$

As for the second term, we will need

$$\mathcal{J}_k(t) \coloneqq \theta_k'(-1)h(-1,t) = \theta_k'(-1)\sum_{i=1}^{s-1}\chi(b_i(t))a_i(t)(-1 - b_i(t)). \tag{19}$$

Using (10), (13) and the above calculations, we derive

$$\begin{aligned}
&p_m\partial_t\widehat{w}(m,t) + \mathcal{H}_m'(t) + \mathcal{J}_m'(t) = \sum_{k=1}^{\infty}\Theta_k'(t)\widehat{\phi_k}(m) \\
&= -n\widehat{\phi_k}(m)\sum_{k=1}^{\infty}\int_{D^\varepsilon} w(b,t)\phi_k(b)\mu_0(b,t)db + \int_{D^\varepsilon}\partial_b w(b,t)\phi_k'(b)\mu_2(b,t)db,
\end{aligned} \tag{20}$$

where $\mu_0$ and $\mu_2$ are defined by the following positive distributions ($n$ can be finite)

$$\begin{aligned}
\mu_0(b,t) &= \frac{1}{n}\sum_{i=1}^{n}\delta(b - b_i(t)), \\
\mu_2(b,t) &= \frac{1}{n}\sum_{i=1}^{n}|a_i(t)|^2\delta(b - b_i(t)).
\end{aligned} \tag{21}$$

Apply the equality $\sum_{k=1}^{\infty}\phi_k(x)\phi_k(y) = \delta(x-y)$ to (20), we find

$$\begin{aligned}
&\widehat{\phi_k}(m)\sum_{k=1}^{\infty}\int_{D^\varepsilon} w(b,t)\phi_k(b)\mu_0(b,t)db \\
&= \int_{D^\varepsilon}\int_D w(b,t)\sum_{k=1}^{\infty}\phi_k(b)\phi_k(b')\mu_0(b,t)\theta_m(b')db'db \\
&= \int_{D^\varepsilon}\int_D w(b,t)\delta(b-b')\mu_0(b,t)\theta_m(b')db'db \\
&= \int_D w(b',t)\mu_0(b',t)\theta_m(b')db' = \widehat{w\mu_0}(m,t).
\end{aligned}$$

Similarly,

$$\begin{aligned}
&\widehat{\phi_k}(m)\sum_{k=1}^{\infty}\int_{D^\varepsilon}\partial_b w(b,t)\phi_k'(b)\mu_2(b,t)db\\
&=\int_{D^\varepsilon}\int_D \partial_b w(b,t)\sum_{k=1}^{\infty}\phi_k'(b)\phi_k(b')\mu_2(b,t)\theta_m(b')db'db\\
&=\int_{D^\varepsilon}\int_D \partial_b w(b,t)\delta'(b-b')\mu_2(b,t)\theta_m(b')db'db\\
&=\int_D \theta_m(b')\delta'(b-b')db'\int_{D^\varepsilon}\partial_b w(b,t)\mu_2(b,t)db\\
&=\int_D \partial_b w(b',t)\mu_2(b',t)\theta_m'(b')db'.
\end{aligned}$$

Therefore (20) can be further reduced to

$$\partial_t\widehat{w}(m,t)=-\frac{1}{p_m}(\mathcal{H}_m'(t)+\mathcal{J}_m'(t))-\frac{n}{p_m}\widehat{w\mu_0}(m,t)-\frac{n}{p_m}\int_D\partial_b w(b',t)\mu_2(b',t)\theta_m'(b')db'. \quad (22)$$

Now we provide an estimate for the above equation and show a slow reduction of high-frequency modes in the initial error during the gradient flow.

**Theorem C.12.** *Assume that* $\sup_{1\le i\le n}|a_i(t)|^2$ *is uniformly bounded by* $M>0$ *and the biases* $\{b_i(0)\}$ *are initially equispaced on* $D$*. If* $\widehat{w}(m,0)\neq 0$*, then there exists a constant* $\widetilde{C}>0$ *depending on the initialized loss that*

$$|\widehat{w}(m,t)|>\frac{1}{2}|\widehat{w}(m,0)|,\quad 0\le t\le\frac{p_m|\widehat{w}(m,0)|}{2n\widetilde{C}(m+1)}. \quad (23)$$

*Especially, denote the initial error in the generalized Fourier mode* $\theta_m$ *by* $|\widehat{w}(m,0)|>c'm^{-2}$ *for certain* $c'>0$*, then the error in the generalized Fourier mode* $\theta_m$ *takes at least* $\mathcal{O}(\frac{c'm}{n})$ *time to get reduced by half following gradient decent dynamics.*

*Proof.* We estimate the contribution from each term on the right-hand side of (22).

1. First, there exists a constant $C>0$ that

$$\begin{aligned}
\left|-\frac{n}{p_m}\widehat{w\mu_0}(m,t)\right|&=\left|\frac{n}{p_m}\int_D w(b',t)\mu_0(b',t)\theta_m(b')db'\right|\\
&\le\frac{n}{p_m}\|w(\cdot,t)\|_{C(D)}\|\theta_m\|_{C(D)}\le\frac{Cn}{p_m}.
\end{aligned} \quad (24)$$

2. Since $w\in H^2(D)$, it can be embedded into $C^{1,\alpha}(D)$ compactly, which means $\partial_b w$ is uniformly bounded on $D$, hence there exists a constant $C'$ that

$$\begin{aligned}
\left|-\frac{n}{p_m}\int_D\partial_b w(b',t)\mu_2(b',t)\theta_m'(b')db'\right|&\le\frac{n}{p_m}\|\theta_m'\|_{C(D)}\|\partial_b w\|_{C(D)}\int_D\mu_2(b,t)db\\
&\le\frac{C'Mmn}{p_m}.
\end{aligned}$$

3. Using the definition of $\mathcal{H}_m$ in (18) and $\mathcal{J}_m$ in (19), now we give the upper bounds of $|\mathcal{H}_m(t)-\mathcal{H}_m(0)|$ and $|\mathcal{J}_m(t)-\mathcal{J}_m(0)|$. Since initially all biases are on $D$, thus $\mathcal{H}_m(0)=0$ and $\mathcal{J}_m(0)=0$. Therefore using the boundedness of $\chi$ and $\chi'$, we have

$$\begin{aligned}
|\mathcal{H}_m(t)-\mathcal{H}_m(0)|&=|\theta_m(-1)|\left|\sum_{l=1}^{s(t)-1}a_l(t)(-\chi(b_l(t))+\chi'(b_l(t))(-1-b_l(t)))\right|\\
&\le C''\sqrt{M}|s(t)-1|
\end{aligned} \quad (25)$$

and

$$|\mathcal{J}_m(t) - \mathcal{J}_m(0)| = |\theta'_m(-1)| \left| \sum_{i=1}^{s(t)-1} a_i(t)\chi(b_i(t)(-1-b_i(t)) \right| \leq C'''m\sqrt{M}|s(t)-1|. \tag{26}$$

Now we estimate the number $s(t)$. Because the biases have a finite propagation speed

$$\left|\frac{d}{dt}b_i(t)\right| \leq |a_i| \int_D |h(x,t) - f(x)|dx \leq K \coloneqq \sqrt{2M}\|h(\cdot,0) - f(\cdot)\|_{L^2(D)}.$$

Therefore there are at most $\frac{1}{2}nKt$ initially evenly spaced biases moving into the transition interval. That gives $|s(t)-1| \leq \frac{1}{2}nKt$.

The above estimates imply that there exists a constant $\widetilde{C} > 0$ that

$$\begin{aligned} |\widehat{w}(m,t)| - |\widehat{w}(m,0)| &\geq -\frac{n}{p_m}(C'Mm + C)t - \frac{1}{p_m}\left(C''\sqrt{M} + C'''m\sqrt{M}\right)\frac{1}{2}Knt \\ &\geq -\frac{\widetilde{C}n}{p_m}(m+1)t. \end{aligned} \tag{27}$$

When $\widehat{w}(m,0) \neq 0$, we solve the lower bound of the *half-reduction* time $\tau > 0$ that

$$\frac{1}{2}|\widehat{w}(m,0)| = \frac{\widetilde{C}n}{p_m}(m+1)\tau \quad \Longrightarrow \quad \tau = \frac{p_m|\widehat{w}(m,0)|}{2n\widetilde{C}(m+1)}.$$

In particular, if $|\widehat{w}(m,0)| > c'm^{-2}$ for certain $c' > 0$, the *half-reduction* time is at least $\mathcal{O}(\frac{c'm}{n})$. □

In order to keep a discretized gradient descent method close to the continuous gradient flow, the learning rate or step size should be small. In practice, one typically takes $\Delta t = \mathcal{O}(\frac{1}{n})$, it will take at least $\mathcal{O}(m)$ time steps to reduce the initial error $h(x,0) - f(x)$ in the generalized Fourier mode $\theta_m$ by half. It is also worth noticing that this phenomenon does not depend on the convergence of the trainable parameters.

### C.3 Some improved bounds

A lower bound estimate only provides an optimistic scenario which may not be sharp. In this section, we improve the estimate in Theorem C.12 when the network width and the frequency mode satisfy different scaling laws.

#### C.3.1 Part I

In the first step, we provide an improved estimate for

$$\int_D \partial_b w(b',t)\mu_2(b',t)\theta'_m(b')db' = \frac{1}{n}\sum_{i=1}^n \partial_b w(b_i(t),t)|a_i(t)|^2\theta'_m(b_i(t)).$$

Here we slightly abuse the notation and treat $\partial_b w$ as zero outside $D$. Define the piecewise linear continuous function $\mathcal{A}(\cdot,t) \in C(D)$ that $\mathcal{A}(b_i(t),t) = |a_i(t)|^2$, then we have the following equation using integration by parts,

$$\begin{aligned} &\frac{1}{n}\sum_{i=1}^n \partial_b w(b_i(t),t)|a_i(t)|^2\theta'_m(b_i(t)) - \int_D \partial_b w(b,t)\mathcal{A}(b,t)\theta'_m(b)db \\ =& -\int_D \texttt{disc}(b,t)\partial_b\left[\partial_b w(b,t)\mathcal{A}(b,t)\theta'_m(b)\right]db, \end{aligned}$$

where `disc` is the discrepancy function

$$\texttt{disc}(b,t) = \frac{1}{n}\sum_{i=1}^n \mathbb{1}_{[-1,b)}(b_i(t)) - b$$

and $\mathbb{1}_S$ denotes the characteristic function on the set $S$.

**Lemma C.13.** *Let $\mathcal{V}(t)$ be the total variation of $\partial_b w(b,t)\mathcal{A}(b,t)\theta_m'(b)$, then there exists an absolute constant $C>0$ that*

$$\mathcal{V}(t) \le CV(\mathcal{A})m^2\|h(\cdot,t)-f(\cdot)\|_{L^2(D)}$$

*where $V(\mathcal{A})$ is the total variation of $\mathcal{A}$:*

$$V(\mathcal{A}) = a_1^2(t) + \sum_{i=1}^{n-1}|a_i^2(t)-a_{i+1}^2(t)| + a_n^2(t). \tag{28}$$

*Proof.* The result comes from the fact $\partial_b^2 w(b,t) = h(b,t)-f(b)$, $|\theta_m^{''}(b)| = O(m^2)$, and bounded variation functions form a Banach algebra. □

**Lemma C.14.** *Suppose $\sup_{1\le i\le n}|a_i(t)|^2$ is uniformly bounded by $M$, the total variation of $\mathcal{A}$ is bounded by $M'$, and the initial biases are equispaced distributed, then there exists a constant $C>0$ such that*

$$\left|\int_D \partial_b w(b',t)\mu_2(b',t)\theta_m'(b')db'\right| \le C\|h(\cdot,0)-f(\cdot)\|_{L^2(D)}\left(1+\left(\frac{2}{n}+Kt\right)m^2\right).$$

*The constant $K=\sqrt{2M}\|h(x,0)-f(x)\|_{L^2(D)}$.*

*Proof.* Let $L=\|\theta_m\|_{C(D)}=\mathcal{O}(1)$, we apply integration by parts and there exists a constant $C'>0$ such that

$$\begin{aligned}
&\left|\int_D \partial_b w(b,t)\mathcal{A}(b,t)\theta_m'(b)db\right| \\
&\le \left|\int_D \theta_m(b)\partial_b\left(\partial_b w(b,t)\mathcal{A}(b,t)\right)db\right| + \left|\theta_m(b)\partial_b w(b,t)\mathcal{A}(b,t)\Big|_{\partial D}\right| \\
&\le L\left[\int_D |\partial_b^2 w(b,t)\mathcal{A}(b,t)|db + \int_D |\partial_b w(b,t)||\partial_b\mathcal{A}(b,t)|db + M\|\partial_b w(\cdot,t)\|_{C(D)}\right] \\
&\le L\left[\|\partial_b^2 w(\cdot,t)\|_{L^2(D)}\|\mathcal{A}(\cdot,t)\|_{L^2(D)} + \|\partial_b w(\cdot,t)\|_{C(D)}V(\mathcal{A}) + M\|\partial_b w(\cdot,t)\|_{C(D)}\right] \\
&\le C'\|h(\cdot,t)-f(\cdot)\|_{L^2(D)}(M+M').
\end{aligned} \tag{29}$$

Therefore we have a new estimate:

$$\begin{aligned}
\left|\int_D \partial_b w(b,t)\mathcal{A}(b,t)\theta_m'(b)db\right| &\le C'\|h(\cdot,t)-f(\cdot)\|_{L^2(D)}(M+M') \\
&\quad + \left|\int_D \texttt{disc}(b,t)\partial_b\left[\partial_b w(b,t)\mathcal{A}(b,t)\theta_m'(b)\right]db\right|.
\end{aligned}$$

Notice that this bound will be better than the constant bound in Theorem C.12 if the second term on the right-hand side is relatively small. Next, we characterize the discrepancy function $\texttt{disc}(b,t)$.

$$\begin{aligned}
|\texttt{disc}(b,t)-\texttt{disc}(b,0)| &= \left|\frac{1}{n}\sum_{i=1}^n \mathbb{1}_{[-1,b)}(b_i(t)) - b - \left(\frac{1}{n}\sum_{i=1}^n \mathbb{1}_{[-1,b)}(b_i(0)) - b\right)\right| \\
&= \frac{1}{n}\left|\sum_{i=1}^n\left(\mathbb{1}_{[-1,b)}(b_i(t)) - \mathbb{1}_{[-1,b)}(b_i(0))\right)\right|.
\end{aligned}$$

Because

$$\left|\frac{d}{dt}b_i(t)\right| \le |a_i(t)|\int_D |h(x,t)-f(x)|dx \le K \coloneqq \sqrt{2M}\|h(x,0)-f(x)\|_{L^2(D)}. \tag{30}$$

and within time $t$, the maximum distance of propagation is $Kt$ for each bias. Therefore,

$$\begin{aligned}
\frac{1}{n}\left|\sum_{i=1}^n\left(\mathbb{1}_{[-1,b)}(b_i(t)) - \mathbb{1}_{[-1,b)}(b_i(0))\right)\right| &\le \frac{1}{n}\left|\sum_{i=1}^n\left(\mathbb{1}_{[-1+Kt,b-Kt)}(b_i(0)) - \mathbb{1}_{[-1,b)}(b_i(0))\right)\right| \\
&= \frac{1}{n}\sum_{i=1}^n \mathbb{1}_{[-1,-1+Kt)\cup[b-Kt,b)}(b_i(0)) \le Kt+\frac{1}{n}.
\end{aligned}$$

Therefore, using $|\texttt{disc}(b,0)| \le \frac{1}{n}$ for equispaced biases,

$$\begin{aligned}\left|\int_D \partial_b w(b,t)\mathcal{A}(b,t)\theta_m'(b)db\right| &\le C'\|h(x,t)-f(x)\|_{L^2(D)}(M+M') + \left(\frac{2}{n}+Kt\right)\mathcal{V}(t)\\ &\le \|h(x,0)-f\|_{L^2(D)}(M+M')\left(C'+\left(\frac{2}{n}+Kt\right)C''m^2\right).\end{aligned}$$

□

**Remark C.15.** *If the bound of $V(\mathcal{A})$ can be as large as $\mathcal{O}(nM)$ at the worst case, then we may return to the Theorem C.12. In fact, if $V(\mathcal{A})$ becomes $\mathcal{O}(m)$, we may also have to return to the Theorem C.12.*

### C.3.2 Part II

In this part, we try to optimize the bound for $\mathcal{J}_m(t) - \mathcal{J}_m(0)$:

$$\mathcal{J}_m(t) - \mathcal{J}_m(0) = \theta_m'(-1)h(-1,t) = \theta_m'(-1)\sum_{i=1}^{s-1} a_i(t)\chi(b_i(t))(-1-b_i(t)).$$

The main result is the following estimate.

**Theorem C.16.** *Assume that $\sup_{1\le i=1\le n}|a_i(t)|^2$ is uniformly bounded by $M>0$ and the biases $\{b_i(0)\}_{i=1}^n$ are initially equispaced on $D$, then there exists a constant $C>0$ that*

$$|\mathcal{J}_m(t) - \mathcal{J}_m(0)| \le Cm\sqrt{M}K^2nt^2.$$

*Proof.* The biases are propagating with finite speed that $|\frac{d}{dt}b_i(t)| \le K := \sqrt{2M}\|h(\cdot,0)-f(\cdot)\|_{L^2(D)}$ (see (30)). If the initial biases are *equispaced* distributed on $D$, then $s(t)-1 \le \frac{Knt}{2}$. For each $1 \le i \le s(t)-1$, the bias $b_i(t)$ satisfies

$$|b_i(t)-b_i(0)| \le Kt, \quad \text{and} \quad |b_i(0)-(-1)| \le Kt.$$

Therefore

$$\begin{aligned}\sum_{i=1}^{s(t)-1}\chi(b_i(t))|-1-b_i(t)| &\le \sum_{i=1}^{s(t)-1}|-1-(b_i(0)-Kt)|\\ &\le \sum_{i=1}^{s(t)-1}|-1-b_i(0)| + Kt(s(t)-1)\\ &\le K^2nt^2.\end{aligned}$$

Therefore $|\mathcal{J}_m - \mathcal{J}_m(0)| \le |\theta_m'(-1)|\sqrt{M}K^2nt^2$. □

### C.3.3 Part III

Now we are ready to summarize the updated theorem with the improved bounds.

**Theorem C.17.** *Suppose $\sup_{1\le i\le n}|a_i(t)|^2$ is uniformly bounded by $M$, the total variation of $\mathcal{A}$ (28) is bounded by $M'$, and the initial biases are equally spaced. Let $n \ge m^4$ be sufficiently large, then it takes at least $\mathcal{O}(\frac{m^4|\widehat{w}(m,0)|}{n})$ to reduce the initial error in generalized Fourier mode $|\widehat{w}(m,t)| \le \frac{1}{2}|\widehat{w}(m,0)|$. Especially when $|\widehat{w}(m,0)| > c'm^{-2}$, the half-reduction time is at least $\mathcal{O}(\frac{m^2c'}{n})$.*

*Proof.* Using Lemma C.14, there exists a constant $C''>0$ that

$$\left|\int_D \partial_b w(b',t)\mu_2(b',t)\theta_m'(b')db'\right| \le C''\left(1+\left(\frac{1}{n}+t\right)m^2\right).$$

We only consider the case that $n \ge m$, otherwise we return to Theorem C.12. Recall that in Theorem C.12 that $|\widehat{w\mu_0}(m,t)|$ is uniformly bounded (see (24)) and $|\mathcal{H}_m(t) - \mathcal{H}_m(0)| \le$

$\frac{1}{2}|\theta_m(-1)|\sqrt{M}Knt$ (see (25) and (26)). Combine the estimate in Theorem C.16 and follow the same process as (27), we can find a constant $C''' > 0$ that

$$|\widehat{w}(m,t)| - |\widehat{w}(m,0)| \leq -C''' \frac{n}{p_m} \left( \left(1 + \frac{m^2}{n}\right) t + (m+m^2)t^2 \right). \tag{31}$$

We solve an upper bound for the half-reduction time $\tau$ from the quadratic equation

$$\frac{1}{2}|\widehat{w}(m,0)| = \frac{n}{p_m} C''' \left( \left(1 + \frac{m^2}{n}\right) \tau + (m+m^2)\tau^2 \right). \tag{32}$$

The solution satisfies

$$\tau \geq \frac{p_m}{2C'''n} \frac{|\widehat{w}(m,0)|}{\sqrt{(1+m^2/n)^2 + 2(m+m^2)p_m|\widehat{w}(m,0)|/(C'''n)}}. \tag{33}$$

Let's use the notations $A \prec B$ and $A \succ B$ to represent the relation $A = \mathcal{O}(B)$ and $B = \mathcal{O}(A)$, respective. We find the following regimes:

1. $n \succ m^2$ and $|\widehat{w}(m,0)| \succ \frac{n}{m^6}$, then $\tau = \mathcal{O}\left(m\sqrt{\frac{\widehat{w}(m,0)}{n}}\right)$.
2. $n \succ m^2$ and $|\widehat{w}(m,0)| \prec \frac{n}{m^6}$, then $\tau = \mathcal{O}\left(\frac{m^4}{n}|\widehat{w}(m,0)|\right)$.
3. $m \prec n \prec m^2$ and $|\widehat{w}(m,0)| \succ \frac{1}{nm^2}$, then $\tau = \mathcal{O}\left(m\sqrt{\frac{\widehat{w}(m,0)}{n}}\right)$.
4. $m \prec n \prec m^2$ and $|\widehat{w}(m,0)| \prec \frac{1}{nm^2}$, then $\tau = \mathcal{O}(m^2|\widehat{w}(m,0)|)$.

In the second case, when $n \succ m^4$ is sufficiently large and $|\widehat{w}(m,0)| > c'm^{-2}$, the half-reduction time becomes $\mathcal{O}(\frac{c'm^2}{n})$, which is a better bound than the one in Theorem C.12. □

**Remark C.18.** *If the biases $b_i$ are equally spaced and fixed, the learning dynamics become the gradient flow for the least square problem. Then one can get a simpler version of (22) without the boundary terms and the last term involving $\theta'_m$. Using an argument similar to C.3.1, one can show $\widehat{\mu_0 w}(m,t) \leq C(\frac{1}{m} + \frac{1}{n}) \leq \frac{2C}{m}$, since the highest frequency modes that can be resolved by the grid is $m \leq \frac{n}{2}$. Then it takes at least $\mathcal{O}(m^3)$ steps to reduce the initial error in mode $m$ by half. Hence the full learning dynamics, i.e., involving the bias, while requiring more computation cost in each step, may speed up the convergence. See Fig 15 for an example.*

### C.4 Numerical experiments

In the following, we perform numerical experiments to demonstrate the scaling laws with a different total variation of $|a_i(t)|^2$. The objective function is

$$f(x) = \sin(k\pi x)$$

with $k$ chosen from selected larger frequencies. We set the number of neurons $n = k^\beta$, $\beta \in \{2,3,4\}$ for a selected frequency $k$. The learning rate is selected as $n^{-1}$. The initialization of biases $\{b_i(0)\}_{i=1}^n$ are equispaced and ordered ascendingly. The weights $\{a_i(0)\}_{i=1}^n$ are initialized in the following ways.

A. $a_i(0) = \frac{1}{2}(-1)^i$.

B. $a_i(0) = \frac{1}{2}\cos(i)$.

We record the dynamics of the network (denoted by $h_k$) at exactly frequency $k$ through the projection

$$E_k(t) = \left| \int_D (h_k(x,t) - f(x))f(x)dx \right|.$$

As we will see in the experiments, the total variation in $\mathcal{A}$ is slowly varying in time, so we can summarize the *a priori* theoretical lower bounds and the experimental results of the number of epochs

in the following tables 3 and 4. The initialization (A) has a relatively small total variation, and the experiments agree with the theoretical bounds quite well. However, similar results are observed for initialization (B), which has a relatively large total variation during the training, see Fig 9, 10, 11 for initialization (A) and Fig 12, 13, 14 for initialization (B). One possible explanation is the overestimate using the total variation in (29) which might be unnecessary. As we mentioned in Remark C.18, we record the training dynamics with *fixed* biases, initialization (A), and choose $n = k^4$, see Fig 15. The result matches the argument in Remark C.18. For comparison purposes, we additionally demonstrate an example with `Adam` optimizer, which shows a similar scaling relation as the `GD` optimizer at the initial training stage, see Fig 15.

All these tests show a consistent phenomenon, the higher the frequency, the slower the learning dynamics.

Table 3: Theoretical lower bounds

| | $TV(\mathcal{A})$ | $\beta = 2$ | $\beta = 3$ | $\beta = 4$ |
|---|---|---|---|---|
| Init A | $\mathcal{O}(1)$ | $\mathcal{O}(k)$ | $\mathcal{O}(k^{1.5})$ | $\mathcal{O}(k^2)$ |
| Init B | $\mathcal{O}(n)$ | $\mathcal{O}(k)$ | $\mathcal{O}(k)$ | $\mathcal{O}(k)$ |

Table 4: Experimental fitted results

| | $TV(\mathcal{A})$ | $\beta = 2$ | $\beta = 3$ | $\beta = 4$ |
|---|---|---|---|---|
| Init A | $\mathcal{O}(1)$ | $\mathcal{O}(k^{1.61})$ | $\mathcal{O}(k^{1.82})$ | $\mathcal{O}(k^{1.87})$ |
| Init B | $\mathcal{O}(n)$ | $\mathcal{O}(k^{1.59})$ | $\mathcal{O}(k^{1.75})$ | $\mathcal{O}(k^{1.90})$ |

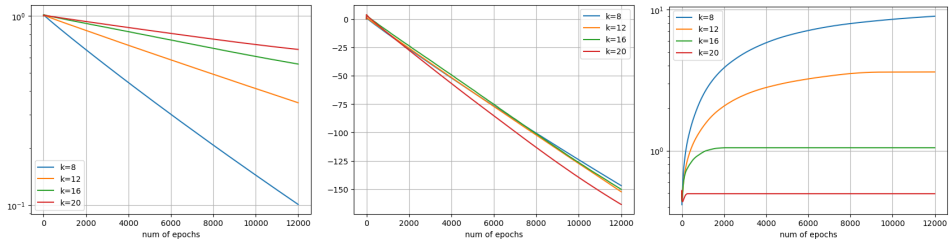


Figure 9: Experiment for initialization (A) and $\beta = 4$. Left: the graphs of $E_k(t)$. Middle: the graphs of $k^{1.87} \ln(E_k(t))$. Right: the total variations of $\mathcal{A}$.

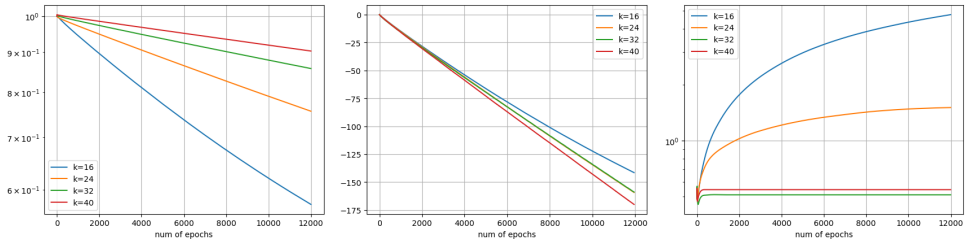


Figure 10: Experiment for initialization (A) and $\beta = 3$. Left: the graphs of $E_k(t)$. Middle: the graphs of $k^{1.82} \ln(E_k(t))$. Right: the total variations of $\mathcal{A}$.

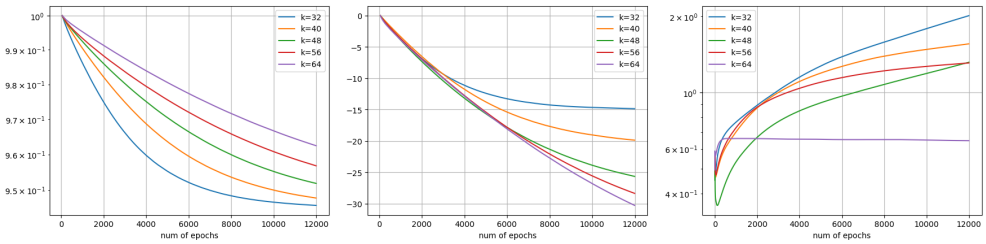


Figure 11: Experiment for initialization (A) and $\beta = 2$. Left: the graphs of $E_k(t)$. Middle: the graphs of $k^{1.61} \ln(E_k(t))$ (fitting first 2000 epochs only). Right: the total variations of $\mathcal{A}$.

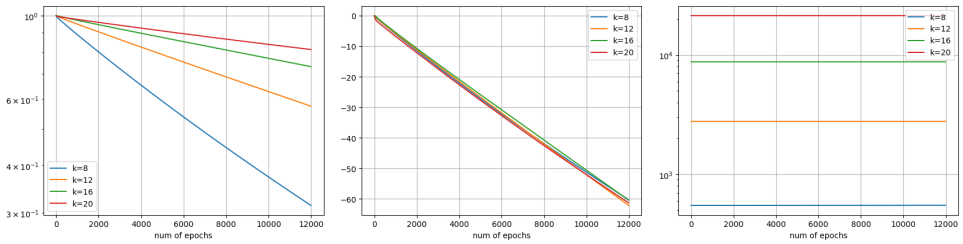


Figure 12: Experiment for initialization (B) and $\beta = 4$. Left: the graphs of $E_k(t)$. Middle: the graphs of $k^{1.90} \ln(E_k(t))$ (fitting first 2000 epochs only). Right: the total variations of $\mathcal{A}$.

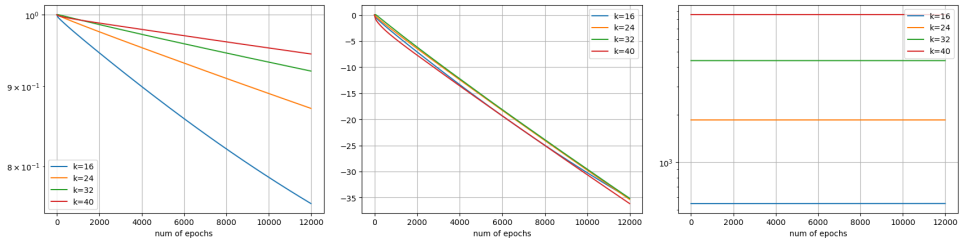


Figure 13: Experiment for initialization (B) and $\beta = 3$. Left: the graphs of $E_k(t)$. Middle: the graphs of $k^{1.75} \ln(E_k(t))$. Right: the total variations of $\mathcal{A}$.

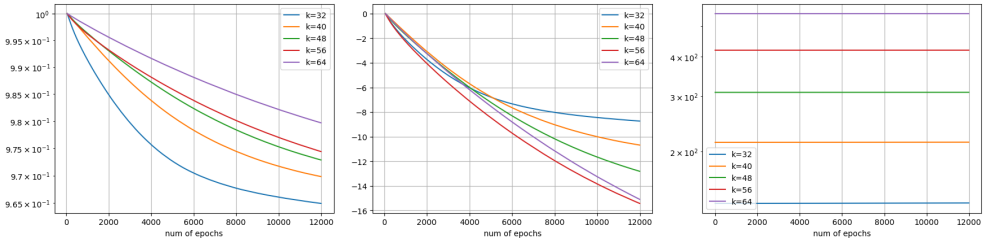


Figure 14: Experiment for initialization (B) and $\beta = 2$. Left: the graphs of $E_k(t)$. Middle: the graphs of $k^{1.59} \ln(E_k(t))$ (fitting first 2000 epochs only). Right: the total variations of $\mathcal{A}$.

### C.5 Further remarks

#### C.5.1 Initial distribution of biases

If the initial biases are uniformly distributed instead of equispaced, the previous estimates need to be modified. In particular, the upper bound of $s(t) - 1$ will become $\frac{Knt}{2} + \mathcal{O}_p(\sqrt{Knt})$ using the Chebyshev inequality. The discrepancy of $\{b_i(0)\}_{i=1}^n$ will be also updated to $\mathcal{O}_p(n^{-1/2})$. Then we

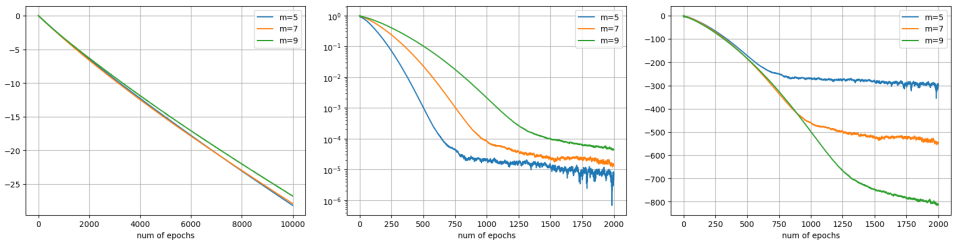


Figure 15: Additional experiment for initialization (A) and $\beta = 4$. Left: Graphs of $k^{3.5}\ln(E_k(t))$ for $k = 5, 7, 9$ with *fixed* equispaced biases, trained by `GD`. Middle: Graphs of $E_k(t)$ for $k = 5, 7, 9$, trained by `Adam`. Right: Graphs of $k^2 \ln E_k(t)$ for $k = 5, 7, 9$, trained by `Adam`.

have the following modified estimates:

$$\begin{aligned}
|\mathcal{H}_m(t) - \mathcal{H}_m(0)| &\leq \frac{1}{2}|\theta_m(-1)|\sqrt{M}(nKt + \mathcal{O}_p(\sqrt{nKt})),\\
|\mathcal{J}_m(t) - \mathcal{J}_m(0)| &\leq |\theta'_m(-1)|\sqrt{M}Kt(Knt + \mathcal{O}_p(\sqrt{Knt})),\\
\left|\int_D \partial_b w(b', t)\mu_2(b', t)\theta'_m(b')db'\right| &\leq C''\left(1 + \left(t + \mathcal{O}_p\left(\frac{1}{\sqrt{n}}\right)\right)m^2\right),
\end{aligned}$$

and (31) becomes

$$|\widehat{w}(m,t)| - |\widehat{w}(m,0)| \underset{p}{\leq} -C'''\frac{n}{p_m}\left(\left(1 + \frac{m^2}{\sqrt{n}}\right)t + (m + m^2)t^2 + (1 + mt)\sqrt{\frac{t}{n}}\right).$$

In particular, when $n \succ m^4$ and $|\widehat{w}(m,0)| > c'm^{-2}$, the half-reduction time is still the same $\mathcal{O}_p(m^2c'/n)$ as Theorem C.17. A similar probabilistic estimate can be derived for initial biases sampled from a continuous probability density function which is bounded from below and above by positive constants.

### C.5.2 Activation function

The regularity of the activation function plays a crucial role in the analysis. In general, using a smoother activation function, which leads to a faster spectrum decay of the corresponding Gram matrix, will take an even longer time to eliminate higher frequencies. For instance, if the activation function is chosen as $\frac{1}{p!}\sigma^p(x)$, $p \geq 1$, where $\sigma$ is the `ReLU` activation function, then a similar analysis will show that if $n \succ m^{p+3}$, then under the assumption of Theorem C.17, the *half-reduction* time of "frequency" $m$ is at least $\mathcal{O}(\frac{m^{2p+2}}{n}|\widehat{w}(m,0)|)$ in the Theorem C.17. This also implies that using a shallow neuron network with smooth activation functions will be even worse to learn and approximate high-frequency information by minimizing the $L^2$ error or mean-squared error (`MSE`).

In the following, we perform a simple numerical experiment to validate our conclusion. We set the objective function as the Fourier mode $f(x) = \sin(m\pi x)$ on $D$, $m \in \mathbb{N}$ and use the activation functions $\texttt{ReLU}^p(x) := \frac{1}{p!}\sigma^p(x)$, $p = 1, 2$ to train the shallow neuron network $h_{m,p}(x, t)$ to approximate $f(x)$, respectively. The number of neurons $n = 10^4$. We record the the *error* of the Fourier mode

$$E_{m,p}(t) := \left|\int_D (h(x,t) - f(x))f(x)dx\right|$$

at each iteration. The errors are shown in Figure 16 for $m = 5, 7, 9$. We can observe that the decay rates of `ReLU` and $\texttt{ReLU}^2$ are $\mathcal{O}(m^{-2})$ and $\mathcal{O}(m^{-3})$ roughly.

### C.5.3 Boundedness of weights

One may notice that the requirement of weights $\sup_{i\geq 1}|a_i(t)|^2 \leq M$ for all $t > 0$ can be relaxed to $0 \leq t \leq \tau$, where $\tau$ denotes the lower bound of half-reduction time in Theorem C.12 or Theorem C.17. When $n \succ m$ in Theorem C.12 or $n \succ m^2$ in Theorem C.17, such requirement can be relaxed to only the initial condition $\sup_{i\geq 1}|a_i(0)|^2 \leq M$.

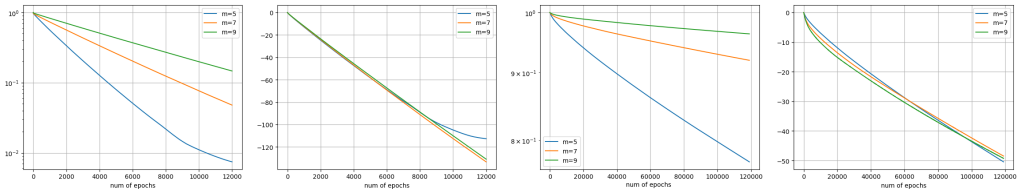

Figure 16: The comparison of ReLU, ReLU$^2$ for the approximation to $f(x) = \sin(m\pi x)$. From left to right, the figures are $E_{m,1}(t)$, $m^{1.95}\ln(E_{m,1}(t))$, $E_{m,2}(t)$, $m^{3.25}\ln(E_{m,2}(t))$.

# D Rashomon sets of shallow neural networks

## D.1 Proof of Theorem 4.1

*Proof.* Let $g \in C_0^2(D)$ that solves $\Delta g(\boldsymbol{x}) = f(\boldsymbol{x})$ with Dirichlet boundary condition.

$$\langle \Delta h(\boldsymbol{x}), g(\boldsymbol{x})\rangle = \frac{1}{n}\sum_{j=1}^{n} X_j, \quad X_j \coloneqq a_j \int_{\boldsymbol{w}_j\cdot\boldsymbol{x}=b_j} g(\boldsymbol{x}) dH_{d-1}(\boldsymbol{x}).$$

The random variables $X_j$ are i.i.d and bounded by $[-A\kappa, A\kappa]$ where $\kappa$ is an absolute constant defined by

$$\kappa \coloneqq \sup_{(\boldsymbol{w}_j,b_j)\in\mathbb{S}^{d-1}\times[-1,1]} \int_{\boldsymbol{w}_j\cdot\boldsymbol{x}=b_j} g(\boldsymbol{x}) dH_{d-1}(\boldsymbol{x}).$$

Then use Hoeffding's inequality,

$$\mathbb{P}\left[\frac{1}{n}\sum_{j=1}^{n} X_j - \mathbb{E}[X_j] \geq t\right] \leq \exp\left(-\frac{nt^2}{2A^2\kappa^2}\right).$$

Especially if $\mathbb{E}(a_j) = 0$ hence $\mathbb{E}(X_j) = 0$, then

$$\mathbb{P}\left[\langle \Delta h(\boldsymbol{x}), g(\boldsymbol{x})\rangle \geq t\right] \leq \exp\left(-\frac{nt^2}{2A^2\kappa^2}\right).$$

Using Green's formula,

$$\langle \Delta h(\boldsymbol{x}), g(\boldsymbol{x})\rangle - \langle h(\boldsymbol{x}), \Delta g(\boldsymbol{x})\rangle = \int_{\partial D} (\partial_n h(\boldsymbol{x}) f(\boldsymbol{x}) - \partial_n f(\boldsymbol{x}) h(\boldsymbol{x}))\, ds = 0,$$

then using the network to approximate $\Delta g = f$ is difficult if $\kappa$ is small in the sense that

$$\begin{aligned}\mathbb{P}\left[\|h(\boldsymbol{x}) - \Delta g(\boldsymbol{x})\|_{L^2(D)} \leq \varepsilon\|\Delta g\|_{L^2(D)}\right] &\leq \mathbb{P}\left[\langle h(\boldsymbol{x}), \Delta g(\boldsymbol{x})\rangle \geq (1-\varepsilon)\|\Delta g\|^2_{L^2(D)}\right] \\ &\leq \exp\left(-\frac{n(1-\varepsilon)^2\|\Delta g\|^4_{L^2(D)}}{2A^2\kappa^2}\right).\end{aligned}$$

Here we have used the fact that $\|h(\boldsymbol{x}) - \Delta g(\boldsymbol{x})\|_{L^2(D)} \leq \varepsilon\|\Delta g\|_{L^2(D)}$ implies both $\|h\|_{L^2(D)} \geq (1-\varepsilon)\|\Delta g\|_{L^2(D)}$ and

$$\langle h, \Delta g\rangle \geq \frac{1-\varepsilon^2}{2}\|\Delta g\|^2_{L^2(D)} + \frac{1}{2}\|h\|^2_{L^2(D)} \geq (1-\varepsilon)\|\Delta g\|^2_{L^2(D)}.$$

□

## D.2 Discussion on bounded activation function

In this section, we discuss about the Rashomon set for bounded activation function instead of ReLU. We consider a more general setting of the parameter space: $a_i$ are mean-zero i.i.d sub-Gaussian random variables that

$$\mathbb{P}[|a_i| > t] < 2e^{-mt^2}, \quad i \in [n]$$

for some $m > 0$. Then we have the following estimate for the Rashomon set by following a similar idea for the proof of Theorem 4.1.

**Theorem D.1.** *Assuming the same network structure as Theorem 4.1 and $\sigma$ as an odd bounded activation function that*

$$-1 \le \sigma(t) \le 1, \quad \sigma'(t) > 0, \quad \forall\, t \in \mathbb{R}, \tag{34}$$

*then the Rashomon set's measure*

$$\mathbb{P}[\|h(\boldsymbol{x}) - f(\boldsymbol{x})\|_{L^2(D)} \le \varepsilon \|f\|_{L^2(D)}] \le 2\exp\left(-\frac{Cn(1-\varepsilon)^2\|f\|_{L^2(D)}^4}{4\kappa^2\ell^2\theta^2}\right),$$

*where $\theta = \|a_i\|_{\psi_2}$ is the* Orlicz *norm, $\ell = diam(D)$, and $\kappa$ denotes*

$$\kappa \coloneqq \sup_{(\boldsymbol{w},t)\in\mathbb{S}^{d-1}\times\mathbb{R}} \left| \int_{\{\boldsymbol{x}\cdot\boldsymbol{w}=t, \boldsymbol{x}\in D\}} f(\boldsymbol{x}) dH_{d-1}\boldsymbol{x} \right|.$$

*Proof.* We denote $r_i \coloneqq |\boldsymbol{w}_i|$ and $\ell = \mathrm{diam}(D)$, then let

$$X_i \coloneqq a_i \int_D f(\boldsymbol{x})\sigma(\boldsymbol{w}_i\cdot\boldsymbol{x} - b_i)d\boldsymbol{x} = \frac{a_i}{r_i}\int_{-\ell r_i}^{\ell r_i} \sigma(s-b_i)\int_{\{\boldsymbol{x}\cdot\boldsymbol{w}_i = s\}} f(\boldsymbol{x}) dH_{d-1}\boldsymbol{x} ds.$$

Then $\langle h, f\rangle = \frac{1}{n}\sum_{i=1}^n X_i$ and

$$\mathbb{P}\left[\|h-f\|_{L^2(D)}^2 \le \varepsilon^2\|f\|_{L^2(D)}^2\right] \le \mathbb{P}\left[(1-\varepsilon)\|f\|_{L^2(D)}^2 \le \frac{1}{n}\sum_{i=1}^n X_i\right].$$

Since the random variable $a_i$ is sub-Gaussian, then $X_i$ is also sub-Gaussian by $|X_i| \le 2a_i\ell\kappa$. One can apply the Hoeffding's inequality (see Theorem 2.6.2 [38]) that

$$\mathbb{P}\left[(1-\varepsilon)\|f\|_{L^2(D)}^2 \le \frac{1}{n}\sum_{i=1}^n X_i\right] \le 2\exp\left(\frac{-Cn(1-\varepsilon)^2\|f\|_{L^2(D)}^4}{4\kappa^2\ell^2\theta^2}\right).$$

for certain absolute constant $C$. □

The constant $\kappa$ stands for the largest possible average of $f$ on every hyperplane $\{\boldsymbol{x}\cdot\boldsymbol{w} = t\}$, $t \in \mathbb{R}$. When $f(\boldsymbol{x})$ is oscillatory in all directions, the constant $\kappa$ becomes small. More intuitively speaking, activation function of the form (34) can not feel oscillations in $f$, i.e., $\langle f, \sigma\rangle$ is small due to cancellation. According to the heuristic argument in [29], it also implies that it is relatively difficult to find a neural network with activation function (34) that can approximate highly oscillatory functions well. Or in other words, the optimal set of parameters only occupies an extremely small measure of the parameter space for highly oscillatory functions.

# E Further discussions

## E.1 General case of Gram matrix of two-layer ReLU networks in 1D

When the two-layer `ReLU` network in 1D is

$$f(x) = c + \sum_{i=1}^n a_i\sigma(w_i x - b_i), \quad x \in D \coloneqq [-1,1],$$

where $w_i \in \{+1, -1\}$ obeys the Bernoulli distribution with $p = \frac{1}{2}$. Then the corresponding Gram matrix has the following block structure of continuous kernels

$$\mathcal{G} \coloneqq \begin{pmatrix} \mathcal{G}^{++}(x,y) & \mathcal{G}^{+-}(x,y) \\ \mathcal{G}^{+-}(x,y) & \mathcal{G}^{--}(x,y) \end{pmatrix}$$

where the sub-kernels are

$$\begin{aligned}
\mathcal{G}^{++}(x,y) &= \frac{1}{24}(2-x-y-|x-y|)^2(2-x-y+2|x-y|) \\
\mathcal{G}^{--}(x,y) &= \frac{1}{24}(2+x+y-|x-y|)^2(2+x+y+2|x-y|) \\
\mathcal{G}^{+-}(x,y) &= \frac{1}{48}\left[|x-y| - (x-y)\right]^3, \\
\mathcal{G}^{-+}(x,y) &= \frac{1}{48}\left[|x-y| + (x-y)\right]^3.
\end{aligned}$$

Note the kernels $\mathcal{G}^{+-}(x,y) = \mathcal{G}^{-+}(-x,-y)$ and $\mathcal{G}^{++}(x,y) = \mathcal{G}^{--}(-x,-y)$, suppose $(g_k^+, g_k^-)$ is an eigenfunction of $\mathcal{G}$ for eigenvalue $\lambda_k$, we can obtain:

1. If $\phi_k(x) = g_k^+(x) + g_k^-(-x) \not\equiv 0$, then it is an eigenfunction of $\mathcal{G}_\phi = \mathcal{G}^{++}(x,y) + \mathcal{G}^{+-}(x,-y)$ for eigenvalue $\lambda_k$.
2. If $\psi_k(x) = g_k^+(x) - g_k^-(-x) \not\equiv 0$, then it is an eigenfunction of $\mathcal{G}_\psi = \mathcal{G}^{++}(x,y) - \mathcal{G}^{+-}(x,-y)$ for eigenvalue $\lambda_k$.

The kernel $\mathcal{G}_\phi \in C^2(D \times D)$ is

$$\mathcal{G}_\phi(x,y) = \frac{1}{12}(|x-y|^3 + |x+y|^3 + 4 + 12xy - 6(x+y) - 6xy(x+y)).$$

Based on the above observation, it is straightforward to derive the following theorem.

**Theorem E.1.** *If the two kernels $\mathcal{G}_\phi$ and $\mathcal{G}_\psi$ do not allow common eigenvalues, then $(g_k^+, g_k^-)$ is an eigenfuntion of $\mathcal{G}$, then they satisfy either $g_k^+(x) = g_k^-(x)$ or $g_k^+(x) = g_k^-(-x)$.*

**Remark E.2.** *The kernel $K_\alpha = |x-y|^\alpha$ has been studied in [3] for $\alpha = 1$, where the eigenvalues have a leading positive term and all of the rest eigenvalues are negative and decay as $\frac{c}{(2k+1)^2}$. Consider the eigenvalue for $|x-y|^3$, we need to find*

$$\lambda h(x) = \int_{-1}^{x} (x-y)^3 h(y)dy + \int_{x}^{1} (y-x)^3 h(y)dy$$

*by differentiating the above equation 4 times, we get $f^{(4)} = \frac{12}{\lambda} h(x)$, let $\omega^4 = \frac{12}{\lambda}$, then the solution consists of the basis*

$$\sum_{k=0}^{3} A_k \exp(\omega e^{\frac{2\pi i k}{4}} x).$$

*Thus solving the eigensystem is equivalent to solving a $4 \times 4$ matrix $\det(M) = 0$ for $\omega$. Similar arguments hold for the Hankel kernel $|x+y|^3$, they share the same basis. The exact values are quite expensive to compute.*

Now we apply the same idea for $\mathcal{G}_\phi$, by the differentiation technique in Lemma A.1, we arrive at the same form:

$$\phi_k(x) = \sum_{l=0}^{3} c_l \exp(\omega e^{\frac{2\pi i l}{4}} x),$$

where $\omega^4 = \frac{2}{\lambda}$, here $\lambda > 0$, thus we choose $\omega \in \mathbb{R}^+$ and the basis are more explicit:

$$\phi_k(x) = c_0 \cosh(\omega x) + c_1 \sinh(\omega x) + c_2 \cos(\omega x) + c_3 \sin(\omega x)$$

The eigenvalues $\lambda_k$ can be computed in a similar way as in Lemma A.1 and there are constants $c_1, c_2 > 0$ that $c_1 k^{-4} \le \lambda_k \le c_2 k^{-4}$.

### E.2 Leaky ReLU activation function

For the leaky ReLU activation function with parameter $\alpha \in (0,1)$, $\sigma_\alpha(x) = \sigma(x) - \alpha\sigma(-x)$, we can derive the Gram matrix $G_\alpha$:

$$\begin{aligned} G_{\alpha,ij} &= \int_{-1}^{1} \sigma_\alpha(x-b_i)\sigma_\alpha(x-b_i)dx \\ &= \int_{-1}^{1} (\sigma(x-b_i) - \alpha\sigma(-x+b_i))(\sigma(x-b_j) - \alpha\sigma(-x+b_j))dx \\ &= \mathcal{G}(b_i,b_j) + \alpha^2\mathcal{G}(-b_i,-b_j) - \frac{\alpha}{6}|b_i - b_j|^3. \end{aligned}$$

Then we can derive the following estimate for the eigenvalue for $G_\alpha$. Let the kernel $\mathcal{G}_\alpha(x,y) \coloneqq \mathcal{G}(x,y) + \alpha^2\mathcal{G}(-x,-y) - \frac{\alpha}{6}|x-y|^3$.

**Theorem E.3.** *Suppose $b_i$ are quasi-evenly spaced on $[-1,1]$, $b_i = -1 + \frac{2(i-1)}{n} + o\left(\frac{1}{n}\right)$. Let $\lambda_1 \geq \lambda_2 \geq \cdots \geq \lambda_n \geq 0$ be the eigenvalues of the Gram matrix $G_\alpha$ then $|\lambda_k - \frac{n}{2}\mu_{\alpha,k}| \leq C$ for some constant $C = \mathcal{O}(1)$, where $\mu_{\alpha,k} = \mathcal{O}(\frac{(\alpha-1)^2}{k^4})$ is the $k$-th eigenvalue of $\mathcal{G}_\alpha$.*

*Proof.* Let the kernel $\mathcal{G}_\alpha(x,y) \coloneqq \mathcal{G}(x,y) + \alpha^2\mathcal{G}(-x,-y) - \frac{\alpha}{6}|x-y|^3$, then following the same idea as Lemma A.1, if $\psi_{\alpha,k}$ is an eigenfunction of $\mathcal{G}_\alpha$ for the eigenvalue $\mu_{k,\alpha}$, we have

$$\psi^{(4)}_{\alpha,k} = \frac{(\alpha-1)^2}{\mu_k}\psi_{\alpha,k}.$$

Let $w_{\alpha,k} = \sqrt{|1-\alpha|}\mu_k^{-\frac{1}{4}}$, then equivalently we obtain the following equation for $w_{\alpha,k}$:

$$\begin{aligned}
&(P_{0,\alpha}(w_{\alpha,k}) + P_{1,\alpha}(w_{\alpha,k})\cos(2w_{\alpha,k}) + P_{2,\alpha}(w_{\alpha,k})\sin(2w_{\alpha,k}))\\
&+ \tanh(w_{\alpha,k})\,(Q_{0,\alpha}(w_{\alpha,k}) + Q_{1,\alpha}(w_{\alpha,k})\cos(2w_{\alpha,k}) + Q_{2,\alpha}(w_{\alpha,k})\sin(2w_{\alpha,k}))\\
&+ \tanh^2(w_{\alpha,k})\,(R_{0,\alpha}(w_{\alpha,k}) + R_{1,\alpha}(w_{\alpha,k})\cos(2w_{\alpha,k}) + R_{2,\alpha}(w_{\alpha,k})\sin(2w_{\alpha,k})) = 0,
\end{aligned}$$

where $P_{i,\alpha}, Q_{i,\alpha}, R_{i,\alpha}$, $i = 0,1,2$ are polynomials of $w_{\alpha,k}$ of degree $\leq 4$. Set $A_\alpha(x) = (-36\alpha^4 + 42\alpha^5 - 12\alpha^6)x^2$ and $B_\alpha(x) = (8\alpha^4 - 8\alpha^5 + 2\alpha^6)x^4$, then

$$\begin{aligned}
P_{0,\alpha}(x) &= \frac{3}{2} + 6\alpha^2 - 6\alpha^3 + \frac{3}{2}\alpha^4 + A_\alpha(x) + B_\alpha(x)\\
P_{1,\alpha}(x) &= P_{0,\alpha}(x) - 3\\
P_{2,\alpha}(x) &= -3\alpha^2(\alpha^2 - 3\alpha + 3)x + 2\alpha^2(\alpha-2)(2 - 9\alpha^2 + 6\alpha^3)x^3\\
Q_{0,\alpha}(x) &= 2\alpha^2 x(-18 + 15\alpha - 42\alpha^2 - 57\alpha^3 + 18\alpha^4 + (12\alpha^2 - 14\alpha^3 + 4\alpha^4)x^2)\\
Q_{1,\alpha}(x) &= 2\alpha^2 x(9 - 6\alpha + 45\alpha^2 - 18\alpha^4 + (8 + 4\alpha + 24\alpha^2 - 28\alpha^3 + 8\alpha^4)x^2)\\
Q_{2,\alpha}(x) &= -12\alpha^2 x^2(-4 + 3\alpha - 10\alpha^2 + 13\alpha^2 + 4\alpha^4)\\
R_{0,\alpha}(x) &= \frac{1}{2}\left[3 - 24\alpha^2 + 12\alpha^3 + 111\alpha^4 - 144\alpha^5 + 48\alpha^6\right] - A_\alpha(x) + B_\alpha(x)\\
R_{1,\alpha}(x) &= \frac{1}{2}\left[-3 + 48\alpha^2 - 36\alpha^2 - 105\alpha^4 + 144\alpha^5 - 48\alpha^6\right] - A_\alpha(x) + B_\alpha(x)\\
R_{2,\alpha}(x) &= \alpha^2(27 - 21\alpha - 87\alpha^2 + 114\alpha^3 - 36\alpha^4)x + \alpha^2(8 - 4\alpha - 12\alpha^2 + 14\alpha^3 - 4\alpha^4)x^2.
\end{aligned}$$

We can rewrite the equation as

$$Z_{0,\alpha}(w_{\alpha,k}) + Z_{1,\alpha}(w_{\alpha,k})\cos(2w_{\alpha,k}) + Z_{2,\alpha}(w_{\alpha,k})\sin(2w_{\alpha,k}) = 0,$$

where $Z_{0,\alpha} = P_{0,\alpha} + \tanh(w_{\alpha,k})Q_{0,\alpha} + \tanh^2(w_{\alpha,k})R_{0,\alpha}$, $Z_{1,\alpha} = P_{1,\alpha} + \tanh(w_{\alpha,k})Q_{1,\alpha} + \tanh^2(w_{\alpha,k})R_{1,\alpha}$ and $Z_{2,\alpha} = P_{2,\alpha} + \tanh(w_{\alpha,k})Q_{2,\alpha} + \tanh^2(w_{\alpha,k})R_{2,\alpha}$. It is not hard to show that as $w_{\alpha,k} > 0$, we have $0 < 1 - \tanh(w_{\alpha,k}) \leq 2e^{-2w_{\alpha,k}}$, and there exists a constant $c > 0$ that $\forall\, x > c$,

$$Z_{0,\alpha}(x) + Z_{1,\alpha}(x) > 0, \quad \text{and} \quad Z_{0,\alpha}(x) - Z_{1,\alpha}(x) < 0$$

by computing the sign of leading power in $x$, which implies that there exist roots on the intervals $[n\pi, (n+\frac{1}{2})\pi]$ and $[(n+\frac{1}{2})\pi, (n+1)\pi]$, respectively for sufficiently large $n$. □

The following corollary can be derived by using the Theorem 1 [37]. It shows that the $k$-th eigenvalue grows as $\mathcal{O}((\alpha-1)^2k^{-4})$ when $k$ is sufficently large.

**Corollary E.4.** *When $\{b_i\}_{i=1}^n$ are i.i.d uniformly distributed on $[-1,1]$, then with probability $1-p$ that*

$$|\lambda_k - \frac{n}{2}\mu_{\alpha,k}| \leq C\frac{n}{k^4}\sqrt{\frac{k}{n}}\log p^{-1}.$$

*for certain constant $C > 0$, where $\mu_{\alpha,k} = \mathcal{O}(\frac{(\alpha-1)^2}{k^4})$ is the $k$-th eigenvalue of $\mathcal{G}_\alpha$.*

The leading eigenvalue $\mu_{\alpha,1}$ can be estimated from above using the Hilbert-Schmidt norm of $\mathcal{G}_\alpha$ and also using the Perron-Frobenious theorem [7] (or Krein-Rutman theorem for positive compact operators), one can estimate $\mu_{\alpha,1}$ from below.

**Corollary E.5.** *For any $\alpha \in (0,1)$, the leading eigenvalue $\mu_{\alpha,1} \in [0.941, 2.754]$.*

*Proof.* First, we compute that

$$\begin{aligned} v(x) &:= \int_{-1}^{1} \mathcal{G}_\alpha(x,y)dy \\ &= \frac{(x-1)^2(x^2+6x+17) - 2\alpha(1+6x^2+x^4) + \alpha^2(x+1)^2(x^2-6x+17)}{24}, \end{aligned}$$

then the leading eigenvalue satisfies

$$\mu_{\alpha,1} \geq \frac{\|v\|_{L^2[-1,1]}}{\sqrt{2}} \geq 2\sqrt{\frac{(728 - 323\alpha + 450\alpha^2 - 323\alpha^3 + 728\alpha^4)}{2835}}.$$

Minimize the right-hand side, we find that $\mu_{\alpha,1} \geq 0.941$, $\forall\, \alpha \in [0,1]$, the minimum is achieved around $\alpha = 0.351$. For the upper bound, we compute the Hilbert-Schmidt norm

$$\sqrt{\int_{-1}^{1}\int_{-1}^{1} |\mathcal{G}_\alpha(x,y)|^2 dxdy} = \sqrt{\beta(\Upsilon \cdot (1, \alpha, \alpha^2, \ldots, \alpha^8))} \leq \frac{32}{3\sqrt{15}} \approx 2.754, \quad \alpha \in [0,1],$$

where $\beta = \frac{512}{212837625}$ and

$$\Upsilon = (1370738, -172283, 394834, -98757, 164086, -98757, 394834, -172283, 1370738) \in \mathbb{R}^9,$$

and the maximum is achieved at $\alpha = 1$. □

We should observe that the leading eigenvalue $\mu_{\alpha,1}$ actually is uniformly bounded from below if $\alpha \in (0,1)$. Therefore the decay of eigenvalues is even worse for $\alpha$ close to 1. This somewhat is straightforward since $\alpha \sim 1$ means the loss of nonlinearity and the eigenvalues collapse to zeros except the leading one.

### E.3 Analytic activation functions

For analytic activation functions such as `Tanh` or `Sigmoid`, the Gram matrix is formed by

$$G_{ij} = \int_D \sigma(\boldsymbol{w}_i \cdot \boldsymbol{x} - b_i)\sigma(\boldsymbol{w}_j \cdot \boldsymbol{x} - b_j)d\boldsymbol{x}$$

Particularly, if the weights $|\boldsymbol{w}_i| \leq A < \infty$, then the kernel function can be viewed as

$$\mathcal{G}(\boldsymbol{x}, \boldsymbol{y}) = \int_D \sigma(\boldsymbol{x} \cdot \boldsymbol{z})\sigma(\boldsymbol{y} \cdot \boldsymbol{z})d\boldsymbol{w}, \quad \boldsymbol{x}, \boldsymbol{y} \in [-A, A] \times [-1, 1],$$

where $\boldsymbol{z} := (\boldsymbol{w}, -1) \in \mathbb{R}^{d+1}$. Since the kernel is analytic in both $\boldsymbol{x}$ and $\boldsymbol{y}$, the eigenvalues of the kernel are decaying faster than any polynomial rate [24, 25]. Two examples in 1D are provided in Figure 17.

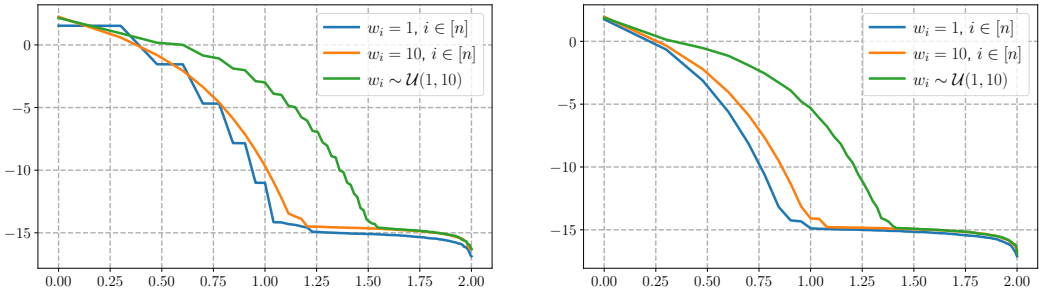


(a) `Tanh`: $\sigma(x) = (e^x - e^{-x})/(e^x + e^{-x})$. (b) `Sigmoid`: $\sigma(x) = 1/(1 + e^{-x})$.

Figure 17: Illustrations of the spectrum of Gram matrices in the one-dimensional case with $n = 100$ for `Tanh` and `Sigmoid` activation functions. The $x$-axis and $y$-axis correspond to $\log_{10} k$ and $\log_{10} \lambda_k$, respectively, for $k \in [n]$. Here, $(b_i)_{i=1}^n$ is evenly spaced in the interval $[-1, 1]$ and $(w_i)_{i=1}^n$ is chosen from one of three cases: $w_i = 1$ for all $i$, $w_i = 10$ for all $i$, or $w_i$ randomly sampled from a uniform distribution $\mathcal{U}(1, 10)$.